

July 2017

Baryon Asymmetry and Gravitational Waves from Pseudoscalar Inflation

Daniel Jiménez,^{a,*} Kohei Kamada,^{b,†} Kai Schmitz,^{a,‡} and Xun-Jie Xu^{a,§}

^a *Max-Planck-Institut für Kernphysik (MPIK), 69117 Heidelberg, Germany*

^b *School of Earth and Space Exploration, Arizona State University, Tempe, AZ 85287, USA*

Abstract

In models of inflation driven by an axion-like pseudoscalar field, the inflaton, a , may couple to the standard model hypercharge via a Chern-Simons-type interaction, $\mathcal{L} \supset a/(4\Lambda) F\tilde{F}$. This coupling results in explosive gauge field production during inflation, especially at its last stage, which has interesting phenomenological consequences: For one thing, the primordial hypermagnetic field is maximally helical. It is thus capable of sourcing the generation of nonzero baryon number, via the standard model chiral anomaly, around the time of electroweak symmetry breaking. For another thing, the gauge field production during inflation feeds back into the primordial tensor power spectrum, leaving an imprint in the stochastic background of gravitational waves (GWs). In this paper, we focus on the correlation between these two phenomena. Working in the approximation of instant reheating, we (1) update the investigation of baryogenesis via hypermagnetic fields from pseudoscalar inflation and (2) examine the corresponding implications for the GW spectrum. We find that successful baryogenesis requires a suppression scale Λ of around $\Lambda \sim 3 \times 10^{17}$ GeV, which corresponds to a relatively weakly coupled axion. The gauge field production at the end of inflation is then typically accompanied by a peak in the GW spectrum at frequencies in the MHz range or above. The detection of such a peak is out of reach of present-day technology; but in the future, it may serve as a smoking-gun signal for baryogenesis from pseudoscalar inflation. Conversely, models that do yield an observable GW signal suffer from the overproduction of baryon number, unless the reheating temperature is lower than the electroweak scale.

*daniel.jimenez@mpi-hd.mpg.de

†kohei.kamada@asu.edu

‡kai.schmitz@mpi-hd.mpg.de

§xunjie.xu@gmail.com

Contents

1	Introduction	2
1.1	Gravitational waves from an anomalous inflaton coupling to gauge fields	2
1.2	Baryogenesis from decaying (hyper)magnetic helicity	4
1.3	Correlation between and successful baryogenesis	6
2	Gauge field production during inflation	8
2.1	Equations of motion for the inflaton and gauge fields	8
2.2	Backreaction on the inflationary dynamics	11
2.3	Hypermagnetic field at the end of inflation	15
3	Gauge field evolution after inflation	16
3.1	From the end of inflation to the onset of the inverse cascade regime	16
3.2	From the onset of the inverse cascade regime to the electroweak crossover	19
3.3	From the electroweak crossover to the present epoch	21
4	Implications for baryon asymmetry and gravitational waves	22
4.1	Baryogenesis from pseudoscalar inflation	23
4.2	High-frequency signal in gravitational waves	27
5	Explicit scenarios based on natural inflation	31
6	Conclusions	36

1 Introduction

In this paper, we are going to study general models of pseudoscalar inflation and their implications for the present-day spectrum of gravitational waves as well as for baryogenesis via primordial hypermagnetic fields around the time of electroweak symmetry breaking (EWSB). In the following, we will review the status of gravitational waves from pseudoscalar inflation in Sec. 1.1 and baryogenesis after primordial magnetogenesis in Sec. 1.2. Readers familiar with both subjects may directly skip to Sec. 1.3, where we outline the philosophy behind our analysis.

1.1 Gravitational waves from an anomalous inflaton coupling to gauge fields

The celebrated detection of gravitational waves (GWs) from a binary black hole merger by the LIGO/Virgo collaboration [1] (see also [2,3]) has literally ringed in the era of gravitational-wave astronomy. In the near future, GW experiments will develop into standard observational tools, allowing us to routinely observe—or better: listen to—a variety of astrophysical phenomena. But also from the perspective of particle physics and cosmology, the observation of GWs bears a huge potential. In particular, the stochastic background of cosmological GWs emitted during

the early universe carries invaluable information on physical processes at extremely high energies that are hard or even impossible to access by other means [4]. Among the different possible mechanisms to generate GWs in the early universe, a prime example is cosmic inflation [5–9], which unavoidably results in the amplification of the quantum vacuum fluctuations of the gravitational field [10–12]. In fact, the direct observation of relic GWs from the epoch of inflation would represent a powerful probe of the earliest moments of our Universe, complementary to other observables that are sensitive to the dynamics of inflation, such as, e.g., the temperature anisotropies of the cosmic microwave background (CMB). Standard single-field slow-roll inflation, however, predicts a present-day GW spectral energy density, $\Omega_{\text{GW}}^0 h^2(f)$, that falls short of the current experimental sensitivity by many orders of magnitude,¹

$$\Omega_{\text{GW}}^0 h^2(f) \sim 10^{-16} \left(\frac{r}{0.1} \right), \quad (1)$$

where the primordial tensor-to-scalar ratio r is bounded from above by the CMB observations of the PLANCK satellite, $r < 0.11$ (95 % C.L.) [15]. This estimate needs to be contrasted with the sensitivity of the Advanced LIGO detector after its first run, $\Omega_{\text{GW}}^0 h^2(f) \sim 10^{-7}$ (95 % C.L., at its most sensitive frequencies, $f \simeq 20 \cdots 86$ Hz) [16]. This sensitivity is certainly an achievement, but still at least nine orders of magnitude away from the expected signal from inflation. Meanwhile, future satellite experiments such as DECIGO [17, 18] and BBO [19, 20] promise to reach sensitivities that might suffice to detect GWs from inflation at $\mathcal{O}(0.1 \cdots 1)$ Hz. But the realization of these experiments is still uncertain and possibly several decades away.

In view of this situation, one is tempted to ask what mechanism could potentially enhance the GW signal from inflation. Here, an interesting possibility — that has recently received renewed attention in the literature [21, 22] — is the boosted production of GWs in models of pseudoscalar inflation [23, 24]. This class of inflationary models is built upon the idea that inflation is driven by the dynamics of a pseudoscalar pseudo-Nambu-Goldstone boson (PNGB) [25, 26].² Such fields correspond to pseudoflat directions in field space, the flatness of which is protected against radiative corrections by an approximate shift symmetry. For this reason, axion-like directions provide a *natural* opportunity to realize slow-roll inflation. The axionic shift symmetry in models of pseudoscalar inflation may, in particular, correspond to the nonlinear realization of an approximate, Peccei-Quinn-like global symmetry G_{global} . Furthermore, if this global symmetry is anomalous under some local gauge symmetry G_{gauge} , the inflaton, a , will couple to the field strength tensor of the corresponding gauge field via an effective Chern-Simons term,

$$\mathcal{L}_{\text{eff}} \supset -\frac{a}{4\Lambda} F_{\mu\nu} \tilde{F}^{\mu\nu}, \quad (2)$$

¹This estimate depends on the reheating temperature, T_{rh} , after inflation. For $T_{\text{rh}} \lesssim \mathcal{O}(10^9)$ GeV, one expects that the GW energy density at frequencies in the $\mathcal{O}(10 \cdots 100)$ Hz range is further diluted — and hence suppressed w.r.t. Eq. (1) — during the stage of expansion dominated by the coherent oscillations of the inflaton field [13, 14].

²The typical example for a PNGB in physics beyond the standard model is the QCD axion [27, 28] in the Peccei-Quinn solution to the strong CP problem [29, 30]. PNGBs in extensions of the standard model are, therefore, also often referred to as axion-like particles or simply axions. In the following, we will use these terms interchangeably.

where $\tilde{F}^{\mu\nu}$ denotes the dual field strength tensor, $\tilde{F}^{\mu\nu} = \frac{1}{2}(-g)^{-1/2} \epsilon^{\mu\nu\sigma\tau} F_{\sigma\tau}$, and where the suppression scale Λ is related to the spontaneous symmetry breaking scale of G_{global} . Similarly, an effective coupling such as in Eq. (2) may arise in compactifications of string theory [31]. In heterotic string theory, e.g., the Green-Schwarz mechanism of anomaly cancellation [32] gives rise to several (model-dependent as well as model-independent) axions that couple to the gauge fields of the theory as in Eq. (2); see [33] for a discussion in the context of pseudoscalar inflation.

The anomalous coupling in Eq. (2) now has important implications for the dynamics of inflation and, eventually, for the present-day spectrum of GWs. To see this, one first has to note that the axion-gauge-field coupling in Eq. (2) results in the explosive production of gauge quanta during inflation [34–36] (see also [37,38]). Depending on the sign of the inflaton velocity, \dot{a} , one of the two helicity modes of the gauge field is exponentially amplified, such that the resulting field configuration is maximally helical. This is a direct consequence of the fact that the time-dependent vacuum expectation value (VEV) of the inflaton field breaks parity invariance during inflation, $\langle \dot{a} \rangle \neq 0$. As the energy transmitted to the gauge field increases, the gauge field begins to back-react on the evolution of the inflaton, effectively contributing another friction term (next to the Hubble friction term) to its equation of motion [39–41]. At the same time, fluctuations in the gauge field configuration result in additional source terms for the primordial scalar and tensor perturbations. Together, these effects have a variety of phenomenological consequences, ranging from modified predictions for various CMB observables [33,42–44], over the production of primordial black holes [44,45], to — and here we finally are — an enhanced spectrum of GWs [21–24].

Recently, it has been pointed out that the GW signal from pseudoscalar inflation may be even amplified to such an extent that it falls into the sensitivity reach of upcoming GW interferometer experiments [21,22]. Here, a particularly promising inflation model appears to be Starobinsky inflation [5], which could potentially lead to observable GWs over a vast range of frequencies. This prediction, however, relies on the assumption of a strong axion coupling, $M_{\text{Pl}}/\Lambda \sim \mathcal{O}(100)$, such that the energy stored in the gauge field begins to dominate the total energy budget towards the end of inflation. As long as the backreaction from the gauge field on the inflationary dynamics remains at a perturbative level at all times, a significantly weaker GW signal is expected.

1.2 Baryogenesis from decaying (hyper)magnetic helicity

The prospect of a sizable GW signal from pseudoscalar inflation entails the question as to what other observable signatures one might hope for. Thanks to the rich phenomenology of this inflationary scenario, it should be possible to correlate the strength of the expected GW signal to other observables. In particular, one would like to know in which case one should either expect a strong or only a rather weak signal in GWs. In this context, an interesting feature of pseudoscalar inflation supplemented by a coupling to gauge fields is the production of primordial gauge fields towards the end of inflation [34–36]. In fact, if the gauge symmetry G_{gauge} is identified with the standard model hypercharge gauge group, $U(1)_Y$, the primordial hypermagnetic fields

generated during inflation might act as seeds for the ubiquitous, intergalactic magnetic fields that permeate our Universe today [46, 47]. Interestingly enough, deficits of secondary cascade photons from TeV blazars have recently been identified, which can be explained by intergalactic magnetic fields [48–54]. Pseudoscalar inflation coupled to the standard model hypercharge sector, therefore, offers an exciting opportunity for *primordial magnetogenesis* [55], which can in principle be tested by more detailed observations of intergalactic magnetic fields.

Moreover, the primordial (hyper)magnetic fields generated during pseudoscalar inflation allow to generate a primordial baryon asymmetry around the time of EWSB [56–58]. The key ingredient in this scenario of baryogenesis is the chiral triangle anomaly in the standard model, which relates changes in the global baryon number B as well as in the global lepton number L to changes in the Chern-Simons numbers in the electroweak sector,³

$$\Delta B = \Delta L = N_g (\Delta N_{\text{CS}}^W - \Delta N_{\text{CS}}^Y) , \quad \Delta N_{\text{CS}}^Y = \frac{g_Y^2}{16\pi^2} \Delta \mathcal{H} . \quad (3)$$

Here, $N_g = 3$ denotes the number of fermion generations in the standard model, while N_{CS}^W and N_{CS}^Y stand for the Chern-Simons numbers associated with the $SU(2)_W$ and $U(1)_Y$ gauge fields, respectively.⁴ Eq. (3) illustrates the well-known fact that $SU(2)_W$ instanton and sphaleron transitions, which correspond to jumps in the non-Abelian Chern-Simons number N_{CS}^W , violate both B and L . But at the same time, Eq. (3) also indicates that both B and L can be generated (or destroyed) by changes in the hypermagnetic helicity \mathcal{H} . And in fact, in the presence of a maximally helical hypermagnetic field generated during pseudoscalar inflation, this is exactly what happens at temperatures around the electroweak scale: The hypermagnetic field is converted into the electromagnetic (EM) field and, as a consequence, the helicity carried by the hypermagnetic field is transferred to the one carried by the EM field. This corresponds to the decay of the net hypermagnetic helicity \mathcal{H} , which, in turn, generates a nonzero baryon number according to the relation in Eq. (3). This mechanism of *baryogenesis via primordial (hyper)magnetic fields* has recently received quite some attention in the literature [61–65] (see also [66, 67]).

In the following, we will adopt the results of [64], which represents the most comprehensive study of this scenario of baryogenesis at the electroweak scale so far. The authors of [64] use recent results from magnetohydrodynamic (MHD) simulations [47, 68] to model the evolution of the magnetic field. In particular, they account for the inverse cascade behavior of the magnetic field below a certain critical temperature, which is characterized by the transfer of power from small scales to large scales [69–71]. Moreover, they include all of the standard model Yukawa interactions as well as the chiral magnetic effect [36, 72]. This is essential to correctly assess the efficiency of $SU(2)_W$ sphaleron processes in washing out the previously generated baryon

³Both baryon and lepton number also exhibit a gravitational anomaly, which can likewise be used to construct scenarios of baryogenesis [59, 60]. In our analysis, the gravitational anomaly will, however, play no role.

⁴Of course, only N_{CS}^W represents a Chern-Simons number in the actual sense, for only the weak isospin gauge sector with non-Abelian gauge group $SU(2)_W$ possesses a topologically nontrivial vacuum structure. In the hypercharge gauge sector, the Chern-Simons number N_{CS}^Y is, by contrast, understood to be related to the hypermagnetic helicity \mathcal{H} , which accounts for topologically nontrivial configurations (knots) of the hypermagnetic gauge field.

number. Finally, the authors of [64] model the gradual conversion of the hypermagnetic field into an EM field during EWSB, i.e., during the electroweak crossover, $\mathbf{B}_Y \rightarrow \mathbf{B}_{\text{EM}}$, in terms of a temperature-dependent weak mixing angle $\theta_W(T)$. In this respect, the analysis in [64] differs drastically from related works, which simply assume that both the generation of baryon number as well as the $SU(2)_W$ sphalerons shut off simultaneously at temperatures around the electroweak scale. As shown in [64], this assumption turns out to be an oversimplification, which basically corresponds to treating the electroweak crossover as a first-order phase transition. In actual fact, the conversion of the hypermagnetic field into the EM field is accompanied by a strong variation in the hypermagnetic helicity and, thus, responsible for an enhanced generation of baryon number. Likewise, one must take into account that also the emerging EM field still participates in redistributing the total baryon number, as it communicates B violation in the left-handed fermions to the right-handed fermions. Taken all together, the authors of [64] find that successful baryogenesis is feasible, as long as the present-day magnetic field exhibits a certain physical strength, B_p^0 , as well as a certain physical correlation length, λ_p^0 ,

$$B_p^0 \sim 10^{-17} \dots 10^{-16} \text{ G}, \quad \lambda_p^0 \sim 10^{-3} \dots 10^{-2} \text{ pc}, \quad (4)$$

and a positive maximal helicity. Note that these values satisfy the relation one expects for magnetic fields that undergo the direct/inverse cascade process, $B_p^0 = 10^{-14} \text{ G} (\lambda_p^0/0.3 \text{ pc})$ [73].⁵ At the same time, they, however, come with an uncertainty of at least one order of magnitude because of the current theoretical uncertainties in modeling the exact evolution of the electroweak crossover. In the following, we will use the numbers in Eq. (4) as a benchmark, keeping in mind that they merely convey an idea of the correct orders of magnitude. Besides that, our final results can be readily carried over to other values of B_p^0 .

1.3 Correlation between and successful baryogenesis

As outlined in Sec. 1.1, pseudoscalar inflation anomalously coupled to the gauge fields of some gauge group G_{gauge} results in the enhanced production of primordial GWs. Here, the identification of G_{gauge} with some non-Abelian group results in the scenario of chromo-natural inflation [74, 75]. The description of an inflaton coupling to non-Abelian fields is, however, slightly more challenging; and hence we shall focus on the Abelian case in this work, for simplicity. Furthermore, among all conceivable Abelian gauge groups that the inflaton could couple to, the standard model hypercharge, $U(1)_Y$, certainly plays a preeminent role. With $U(1)_Y$ being the only Abelian gauge group in the standard model, an inflaton coupling to the hypercharge sector

⁵In this paper, we are going to work in *natural Lorentz-Heaviside units*, in which $\hbar = c_0 = \epsilon_0 = 1$. These are the typical units of particle physics, where the electrical charge e is supposed to be related to the fine structure constant α as $e = \sqrt{4\pi\alpha}$. This means that $1 \text{ G} = 6.91 \times 10^{-20} \text{ GeV}^2 (4\pi\epsilon_0)^{-1/2} (\hbar c_0)^{-3/2} = 1.95 \times 10^{-20} \text{ GeV}^2$. In *natural Gaussian CGS units*, one has by contrast $\hbar = c_0 = 4\pi\epsilon_0 = 1$, such that $e = \sqrt{\alpha}$ and $1 \text{ G} = 6.91 \times 10^{-20} \text{ GeV}^2$. To convert from our units to CGS units, one simply has to replace $1 \text{ G} \rightarrow (4\pi)^{-1/2} \text{ G}$. Meanwhile, the conversion from parsec to inverse GeV is unambiguous and identical in both unit systems, $1 \text{ pc} = 1.56 \times 10^{32} \text{ GeV}^{-1}$.

may be regarded as a *most minimal* departure from the standard model. A coupling to any other gauge symmetry, such as, e.g., $U(1)_{B-L}$, would by contrast require the introduction of new gauge degrees of freedom (DOFs). Moreover, coupling pseudoscalar inflation to the hypercharge sector also offers an intriguing possibility for primordial magnetogenesis, which can be tested by the observations of the present intergalactic magnetic fields, as well as for baryogenesis from the decay of (hyper)magnetic helicity; see the discussion in Sec. 1.2. For these reasons, we deem the identification $G_{\text{gauge}} \rightarrow U(1)_Y$ the most interesting choice. In contrast to any hidden gauge symmetries beyond the standard model, an inflaton coupling to $U(1)_Y$ is slightly less speculative and, at the same time, more predictive in terms of observable consequences.

In this paper, we are, therefore, going to focus on general models of pseudoscalar inflation supplemented by a Chern-Simons-type interaction between the inflaton and the hypermagnetic gauge field. In particular, we are going to address the following two questions:

(1) Under what conditions does pseudoscalar inflation result in a (hyper)magnetic field of just the right magnitude, such that primordial magnetogenesis at the end of inflation sets the stage for successful baryogenesis at the electroweak scale? That is, how does one need to choose the parameters of pseudoscalar inflation in order to satisfy the two conditions in Eq. (4)? In this part of our analysis, we are basically going to update previous studies of *baryogenesis from pseudoscalar inflation* [61,65] (see also [76]). By employing the results presented in [64], we make sure to include several important effects that had been neglected up to this point (such as, e.g., the inverse cascade regime, the chiral magnetic effect, and the role of the standard model Yukawa interactions). In doing so, we will work in the approximation of instant reheating, for simplicity. In principle, both magnetic fields and gravitational waves are also produced during the stage of reheating [76–78]. The correct description of this phase, however, requires a dedicated numerical simulation that includes both nonperturbative particle production and MHD. In particular, one should take into account the backreaction on the gauge field production from the hypercharged particles in the emerging plasma. Such a study is not yet available, which is why we will ignore the details of the reheating phase altogether. On the one hand, the approximation of instant reheating introduces some (perhaps very large) uncertainties into our analysis.⁶ On the other hand, it allows us to remain absolutely model-independent, as far as the concrete dynamics of inflation and reheating are concerned. Against this background, we hope that our analysis may motivate further studies of reheating after pseudoscalar inflation that account for the complicated interplay between gauge field production and the properties of the emerging charged plasma.

⁶The lattice simulation in [76], e.g., indicates a large enhancement of hypermagnetic fields at the stage of reheating. On the contrary, the authors of [78] point out the necessity of a relatively low reheating temperature in order to avoid high electric conductivity, which would otherwise prevent hypermagnetic helicity from developing during reheating. However, a low reheating temperature automatically comes with a large dilution of the hypermagnetic field. From this perspective, one would therefore rather expect a suppression than an enhancement from reheating. In the following, we will evade the (still on-going) debate which of these conclusions is correct and simply neglect any contributions to the hypermagnetic field from reheating. Instead, we will simply focus on the gauge field production during inflation. In this sense, our estimate is a quantitatively conservative one.

(2) What are the implications of successful baryogenesis for the present-day GW spectrum? Assuming that primordial magnetogenesis results in magnetic fields in accord with Eq. (4), is there still a chance to obtain GWs that could be detected in GW experiments in the near future?

To answer these questions, we will now proceed as follows: In Sec. 2, we will first review the production of hypermagnetic fields in models of pseudoscalar inflation. We will discuss in particular the dependence on the suppression scale Λ as well as the backreaction on the inflationary dynamics. In Sec. 3, we will then study the evolution of the primordial hypermagnetic fields from the time of their production all the way to the present epoch. In Sec. 4, we will in turn study the implications for baryogenesis as well as for the GW spectrum. Here, our main interest will be to establish a connection between successful baryogenesis and the expected strength of the GW signal from inflation. In Sec. 5, we will finally illustrate some of our main results numerically by means of a concrete example, based on the original model of natural inflation [25, 26]. Sec. 6 contains our conclusions as well as a brief outlook on how our work could be continued.

2 Gauge field production during inflation

We begin by reviewing the mechanism of gauge field production in models of pseudoscalar inflation [34–36]. This will also serve the purpose to establish our notation and conventions.

2.1 Equations of motion for the inflaton and gauge fields

For an arbitrary model of pseudoscalar inflation coupled to the standard model hypercharge sector via an effective Chern-Simons term, the relevant Lagrangian takes the following form,

$$\mathcal{L} \supset -\frac{1}{2}\partial_\mu a \partial^\mu a - \frac{1}{4}F_{\mu\nu}F^{\mu\nu} - V(a) - \frac{a}{4\Lambda}F_{\mu\nu}\tilde{F}^{\mu\nu}. \quad (5)$$

Here, the field a denotes the axion-like pseudoscalar inflaton; $F_{\mu\nu} = \partial_\mu A_\nu - \partial_\nu A_\mu$ is the field strength tensor belonging to the hypercharge gauge field A_μ ; and $\tilde{F}^{\mu\nu}$ is the dual field strength tensor, $\tilde{F}^{\mu\nu} = \frac{1}{2}(-g)^{-1/2}\epsilon^{\mu\nu\sigma\tau}F_{\sigma\tau}$. For the time being, we remain as model-independent as possible and do not specify the concrete form of the inflaton potential $V(a)$. Only in Sec. 5, we will become more explicit and identify $V(a)$ with the scalar potential of particular models of inflation. The last term in Eq. (5) represents the anomalous Chern-Simons interaction between the inflaton and the hypercharge gauge field. The parameter Λ denotes an effective suppression scale, the magnitude of which is related to the energy scale at which the anomalous coupling is generated. In the following, we will treat it as a free parameter. The combination a/Λ , i.e., the prefactor of the topological term $\frac{1}{4}F_{\mu\nu}\tilde{F}^{\mu\nu}$, may be regarded as an effective, field-dependent vacuum angle in the hypercharge sector, $\theta = a/\Lambda$. If we replaced a by a constant, θ would become unphysical and could be transformed away by a fermion rotation. However, with a being a dynamical field, the vacuum angle θ is physically meaningful; see also [79].

Given the Lagrangian in Eq. (5), one obtains for the homogeneous Friedmann equation,

$$H^2 = \left(\frac{\dot{R}}{R}\right)^2 = \frac{\rho}{3M_{\text{Pl}}^2}, \quad \rho = \frac{1}{2}\dot{a}^2 + V(a) + \frac{1}{2}\langle \mathbf{E}^2 \rangle + \frac{1}{2}\langle \mathbf{B}^2 \rangle. \quad (6)$$

Here, H is the Hubble rate; R denotes the scale factor in the Friedmann-Lemaître-Robertson-Walker metric, $ds^2 = -dt^2 + R^2(t) d\mathbf{x}^2 = -R^2(t) (d\tau^2 - d\mathbf{x}^2)$; ρ represents the total energy density; and $M_{\text{Pl}} = (8\pi G)^{-1/2} = 2.44 \times 10^{18}$ GeV is the reduced Planck mass. \dot{R} stands for the derivative of the scale factor w.r.t. physical time t . Below, we will also encounter derivatives w.r.t. conformal time τ , which will be denoted by a prime. The total energy density ρ can be obtained from the stress-energy tensor. In addition to the usual contributions from the inflaton field, it now also receives contributions from the hyperelectric and hypermagnetic fields \mathbf{E} and \mathbf{B} . We are going to work in radiation gauge, which combines the gauge fixing conditions of Coulomb (or transverse) gauge, $\nabla \cdot \mathbf{A} = 0$, and Weyl (or temporal) gauge, $A_0 = 0$. The fields \mathbf{E} and \mathbf{B} are then related to the components of the hypercharge vector field A_μ as follows,

$$A_\mu = (A_0, \mathbf{A}), \quad \mathbf{E} = -\frac{1}{R^2} \partial_\tau \mathbf{A} = -\frac{1}{R^2} \mathbf{A}', \quad \mathbf{B} = \frac{1}{R^2} \nabla \times \mathbf{A}. \quad (7)$$

\mathbf{E} and \mathbf{B} are understood to represent *physical* field strengths, whereas A_μ is a *comoving* quantity that needs to be determined in dependence of the comoving coordinates $x^\mu = (\tau, \mathbf{x})$. The angle brackets in Eq. (6) denote the expectation values of \mathbf{E}^2 and \mathbf{B}^2 , respectively. During inflation, these expectation values correspond to *quantum mechanical* vacuum expectation values. In order to determine the *classical* field strengths after inflation, we identify these quantum expectation values with the ensemble averages of the classical fields just at the end of inflation,

$$\langle \cdot \rangle_{\text{quantum vacuum}} \xrightarrow{\text{end of inflation}} \langle \cdot \rangle_{\text{classical ensemble}}. \quad (8)$$

Similarly as the Friedmann equation, the equation of motion for the homogeneous inflaton field also turns out to receive corrections in presence of the anomalous axion-gauge-field coupling,

$$\ddot{a} + 3H\dot{a} + \frac{dV}{da} = \frac{1}{\Lambda} \langle \mathbf{E}\mathbf{B} \rangle. \quad (9)$$

Here, the new source term on the right-hand side may be regarded as an additional friction term (next to the usual Hubble friction term, $3H\dot{a}$). In the case of strong gauge field production, the source term eventually dominates over the Hubble friction term, which alters the inflationary dynamics towards the end of inflation [39–41] (see also [21, 22]). As we will see later on, this regime will be less relevant for our purposes, i.e., as long as we require successful baryogenesis.

The dynamics of the vector field are governed by the following wave equation,

$$\square \mathbf{A} = -\mathbf{A}'' + \nabla^2 \mathbf{A} = -\frac{a'}{\Lambda} \nabla \times \mathbf{A}, \quad (10)$$

where the axion-gauge-field coupling induces again a source term on the right-hand side. To find the solution of this equation, it is convenient to perform a Fourier transform and work in momentum space. Upon quantization of the individual Fourier modes, \mathbf{A} may be written as

$$\mathbf{A}(\tau, \mathbf{x}) = \sum_{\lambda=\pm} \int \frac{d^3\mathbf{k}}{(2\pi)^{3/2}} \left[A_\lambda(\tau, \mathbf{k}) \boldsymbol{\epsilon}_\lambda(\mathbf{k}) \hat{a}_\lambda(\mathbf{k}) e^{i\mathbf{k}\mathbf{x}} + \text{h.c.} \right]. \quad (11)$$

Here, $\lambda = \pm$ labels the two possible helicity states; A_{\pm} denote the corresponding mode functions; ϵ_{\pm} are the two polarization vectors; and \hat{a}_{\pm} stand for the corresponding annihilation operators, which annihilate states $|\mathbf{k}, \lambda\rangle$ with 3-momentum \mathbf{k} and polarization λ . The vectors ϵ_{\pm} for given momentum \mathbf{k} form an orthonormal basis in the complex vector space perpendicular to \mathbf{k} ,

$$\epsilon_{\lambda}(\mathbf{k}) \cdot \epsilon_{\lambda'}^*(\mathbf{k}) = \delta_{\lambda\lambda'}, \quad \epsilon_{\lambda}(\mathbf{k}) \cdot \mathbf{k} = 0, \quad i\mathbf{k} \times \epsilon_{\lambda}(\mathbf{k}) = \lambda k \epsilon_{\lambda}(\mathbf{k}), \quad (12)$$

where $k = |\mathbf{k}|$. Meanwhile, the annihilation and creation operators, $\hat{a}_{\lambda}(\mathbf{k})$ and $\hat{a}_{\lambda}^{\dagger}(\mathbf{k})$, satisfy the usual canonical commutation relations, $[\hat{a}_{\lambda}(\mathbf{k}), \hat{a}_{\lambda'}^{\dagger}(\mathbf{k}')] = \delta_{\lambda\lambda'} \delta^{(3)}(\mathbf{k} - \mathbf{k}')$. Inserting the Fourier expansion in Eq. (11) into the equation of motion in Eq. (10) and using the relations in Eq. (12), one then obtains the following mode equations in momentum space,

$$\left[\frac{\partial^2}{\partial \tau^2} + k^2 \left(1 - \frac{x_{\lambda}(\xi)}{x(\tau, k)} \right) \right] A_{\lambda}(\tau, \mathbf{k}) = 0, \quad x(\tau, k) = -k\tau, \quad x_{\lambda}(\xi) = 2\lambda\xi, \quad (13)$$

where we have defined the *instability parameter* ξ as follows,

$$\xi = \frac{1}{2H} \frac{\dot{a}}{\Lambda}. \quad (14)$$

The mode equations are isotropic in momentum space, which is why we will label the mode functions only by their absolute momenta from now on, $A_{\lambda}(\tau, \mathbf{k}) \rightarrow A_{\lambda}^k(\tau)$. The parameter x in Eq. (13) quantifies whether, at a certain conformal time τ , a given mode with wavenumber k has a spatial extent (i.e., physical wavelength $\lambda_p = 2\pi R/k$) larger or smaller than the Hubble radius, H^{-1} . To see this, one simply has to recall that during inflation, i.e., in quasi-de Sitter space, τ is approximately given as $\tau \simeq -1/(RH)$. This readily implies $x \simeq 2\pi H^{-1}/\lambda_p$. The magnitude of x needs to be compared with x_{λ} , which is defined in terms of the instability parameter ξ . The parameter $x_{\lambda} = \lambda\dot{\theta}/H$ in Eq. (13) hence measures the rate of variation of the effective vacuum angle $\theta = a/\Lambda$ in relation to the Hubble rate H . With the above definitions, one also finds that $x_{\lambda}/x = \lambda k_{\text{crit}}/k$, where $k_{\text{crit}} = R\dot{\theta}$ is a certain critical (comoving) momentum scale. From the perspective of gauge field production, the quantities x_{λ} , ξ , and k_{crit} vary only slowly with time. This is a direct consequence of the slow-roll motion of the field a during inflation. When solving the mode equations in Eq. (13), we will, therefore, treat x_{λ} at any given moment in time as a constant. This will provide us with solutions for the vector-field modes that are respectively valid during certain periods of inflation, when x_{λ} takes particular, approximately constant values. Other than that, we will make no further approximations when solving Eq. (13).

From Eq. (13), it is evident that, for $x < |x_{\lambda}|$, the helicity modes corresponding to positive x_{λ} become tachyonically unstable. A positive baryon asymmetry requires a positive (hyper)magnetic helicity [62–64]. In the following, we will therefore consider the case where $\dot{a} > 0$, such that $x_{+} > 0$ and $x_{-} < 0$. In this case, the positive-helicity modes A_{+}^k will be tachyonically unstable at $x < x_{+}$.⁷ Once x has dropped down to values smaller than x_{+} , the modes A_{+}^k begin

⁷Conversely, in the case of negative inflaton velocity, $\dot{a} < 0$, we would have to deal with $x_{-} > 0$ and $x_{+} < 0$. This would result in a negative helicity and, consequently, in a negative baryon asymmetry. For the inflationary dynamics, the sign of the induced helicity does not matter. Moreover, as long as the inflaton potential is invariant under parity, $a \leftrightarrow -a$, the sign of the inflaton velocity does not affect the inflationary dynamics as well.

to exponentially grow. The negative-helicity modes A_-^k experience, by contrast, only a shift in their dispersion relation towards effectively *larger* momenta, $k^2 \rightarrow k^2(1 + k_{\text{crit}}/k)$. They, thus, always stay at the quantum level. For constant ξ , the exact solutions for A_{\pm}^k are given in terms of Whittaker W functions (which are related to confluent hypergeometric functions) [80]. This is because Eq. (13) can be brought into a particular form of Whittaker's equation,

$$\left(\frac{d^2}{dz^2} - \frac{1}{4} + \frac{\kappa_\lambda}{z}\right) A_\lambda^k(z) = 0, \quad z = -2ix = 2ik\tau, \quad \kappa_\lambda = \frac{x_\lambda}{2i} = -i\lambda\xi. \quad (15)$$

We require that the modes A_{\pm}^k reduce to the usual Bunch-Davis solution in the asymptotic past,

$$\lim_{-k\tau \rightarrow \infty} A_\lambda^k(\tau) = \frac{e^{-ik\tau}}{\sqrt{2k}}. \quad (16)$$

With this boundary condition, the Whittaker equation in Eq. (15) has the following solution,

$$A_\lambda^k(\tau) = \frac{e^{\lambda\pi\xi/2}}{\sqrt{2k}} W_{-i\lambda\xi, 1/2}(2ik\tau), \quad (17)$$

where $W_{-i\lambda\xi, 1/2}$ is the Whittaker function $W_{\kappa, \mu}$ with indices $\kappa = \kappa_\lambda = -i\lambda\xi$ and $\mu = 1/2$. This function grows exponentially as a function of τ for $\lambda = +$ and remains oscillatory for $\lambda = -$.

2.2 Backreaction on the inflationary dynamics

In the previous section, we have seen how the axion-induced source term on the right-hand side of Eq. (10) manages to excite vector-field modes with positive helicity; see Eq. (17). We shall now examine the consequence of this nonperturbative gauge field production for the inflationary dynamics. In the presence of a macroscopic gauge field configuration, the Friedmann and Klein-Gordon equations in Eqs. (6) and (9) need to be supplemented by the following expressions,

$$\begin{aligned} \rho_{EE} &= \frac{1}{2} \langle \mathbf{E}^2 \rangle = \frac{1}{2R^4} \int \frac{d^3\mathbf{k}}{(2\pi)^3} \left| \frac{\partial}{\partial\tau} A_+^k \right|^2, \\ \rho_{BB} &= \frac{1}{2} \langle \mathbf{B}^2 \rangle = \frac{1}{2R^4} \int \frac{d^3\mathbf{k}}{(2\pi)^3} k^2 |A_+^k|^2, \\ \rho_{EB} &= \frac{1}{2} \langle \mathbf{E}\mathbf{B} \rangle + \frac{1}{2} \langle \mathbf{B}\mathbf{E} \rangle = -\frac{1}{2R^4} \int \frac{d^3\mathbf{k}}{(2\pi)^3} k \frac{\partial}{\partial\tau} |A_+^k|^2, \end{aligned} \quad (18)$$

where we neglect the vacuum contributions from the negative-helicity modes. The quantities ρ_{EE} and ρ_{BB} have a direct interpretation in the sense that they correspond to the energy densities stored in the hyperelectric and hypermagnetic fields, respectively. The quantity ρ_{EB} is the corresponding cross term. We note that the \mathbf{E} and \mathbf{B} fields do *not* commute at the quantum level, which is why ρ_{EB} is defined as the symmetrized version of $\langle \mathbf{E}\mathbf{B} \rangle$. Technically, the right-hand side of Eq. (9) is understood to correspond to ρ_{EB}/Λ . In the classical limit, the commutator $[\mathbf{E}, \mathbf{B}]$, however, vanishes and ρ_{EB} and $\langle \mathbf{E}\mathbf{B} \rangle$ become equivalent to each other.

The energy densities in Eq. (18) are functions of the inflationary Hubble rate H as well as of the instability parameter ξ ; see Eq. (14). To extract the dependence on these two parameters,

it turns out convenient to rewrite the momentum integrals in Eq. (18) as follows,

$$\rho_{EE} = \mathcal{I}_{EE}(\xi) \frac{e^{2\pi\xi}}{\xi^3} H^4, \quad \rho_{BB} = \mathcal{I}_{BB}(\xi) \frac{e^{2\pi\xi}}{\xi^5} H^4, \quad \rho_{EB} = -\mathcal{I}_{EB}(\xi) \frac{e^{2\pi\xi}}{\xi^4} H^4, \quad (19)$$

with the integral functions \mathcal{I}_{EE} , \mathcal{I}_{BB} and \mathcal{I}_{EB} being defined as

$$\begin{aligned} \mathcal{I}_{EE}(\xi) &= \frac{\xi^3}{8\pi^2} e^{-\pi\xi} \int_0^{x_{UV}} dx x^3 \left| \frac{\partial}{\partial x} W_{\kappa_+, 1/2}(-2ix) \right|^2, \\ \mathcal{I}_{BB}(\xi) &= \frac{\xi^5}{8\pi^2} e^{-\pi\xi} \int_0^{x_{UV}} dx x^3 |W_{\kappa_+, 1/2}(-2ix)|^2, \\ \mathcal{I}_{EB}(\xi) &= \frac{-\xi^4}{8\pi^2} e^{-\pi\xi} \int_0^{x_{UV}} dx x^3 \frac{\partial}{\partial x} |W_{\kappa_+, 1/2}(-2ix)|^2. \end{aligned} \quad (20)$$

Here, we choose a sign convention such that all three functions are positive. The fact that ρ_{EB} actually takes negative values is accounted for by the explicit minus sign in Eq. (19). In principle, the momentum integrals in Eq. (18) are UV-divergent, as they receive vacuum contributions from an infinite number of high-frequency modes (i.e., modes deep inside the Hubble horizon). To regularize this divergence, we introduce a UV cut-off scale, $x_{UV} = k_{UV}/(RH)$, which allows us to integrate over only those modes that are excited above the vacuum level. The natural choice for x_{UV} is consequently $x_{UV} = x_+ = 2\xi$, such that the momentum cut-off k_{UV} coincides with k_{crit} , i.e., the highest wavenumber that still leads to a tachyonic instability in Eq. (13).

In view of Eq. (20), it is also interesting to note that we absorbed the *explicit* time dependence of the vector-field modes $A_{\pm}^k(\tau)$ in Eq. (18) into the integration variable $x = -k\tau$. The remaining time dependence is then canceled by the time dependence of R^{-4} in front of the integrals in Eq. (18). At first glance, this renders all of the three quantities in Eq. (19) constant in time. However, there remains an *implicit* time dependence encoded in the parameters ξ and H , which actually slowly vary during inflation. In the following, we will determine ρ_{EE} , ρ_{BB} , ρ_{EB} at any time t during inflation simply by evaluating Eq. (19) for the respective values of $\xi(t)$ and $H(t)$. If we were to treat the time dependence of ξ and H more carefully, we would have to solve Eqs. (6), (9), and (13) simultaneously. Such an analysis is beyond the scope of this paper.

The advantage of the parametrization in Eq. (19) is that all of the three functions \mathcal{I}_{EE} , \mathcal{I}_{BB} , and \mathcal{I}_{BE} asymptotically approach constant values at $\xi \gg 1$. This is depicted in Fig. 1, where we also demonstrate the sensitivity of the three integral functions to variations in the UV cut-off. As can be seen from Fig. 1, all three functions become insensitive to the exact choice for x_{UV} as soon as they approach their respective asymptotic values. For $\xi \gtrsim 4$, it is, therefore, safe to approximate \mathcal{I}_{EE} , \mathcal{I}_{BB} , and \mathcal{I}_{BE} by the constant values shown in Fig. 1,

$$\rho_{EE} \simeq 1.3 \times 10^{-4} \frac{e^{2\pi\xi}}{\xi^3} H^4, \quad \rho_{BB} \simeq 1.5 \times 10^{-4} \frac{e^{2\pi\xi}}{\xi^5} H^4, \quad \rho_{EB} \simeq -2.6 \times 10^{-4} \frac{e^{2\pi\xi}}{\xi^4} H^4. \quad (21)$$

These results are consistent with the approximate solution for the excited mode functions, $A_{\pm}^k(x) = (2k)^{-1/2} (x/x_+)^{1/4} \exp[\pi x_+/2 - 2\sqrt{xx_+}]$, which is often employed in the literature.

With Eq. (21) at our disposal, we are now able to assess the relative importance of the new

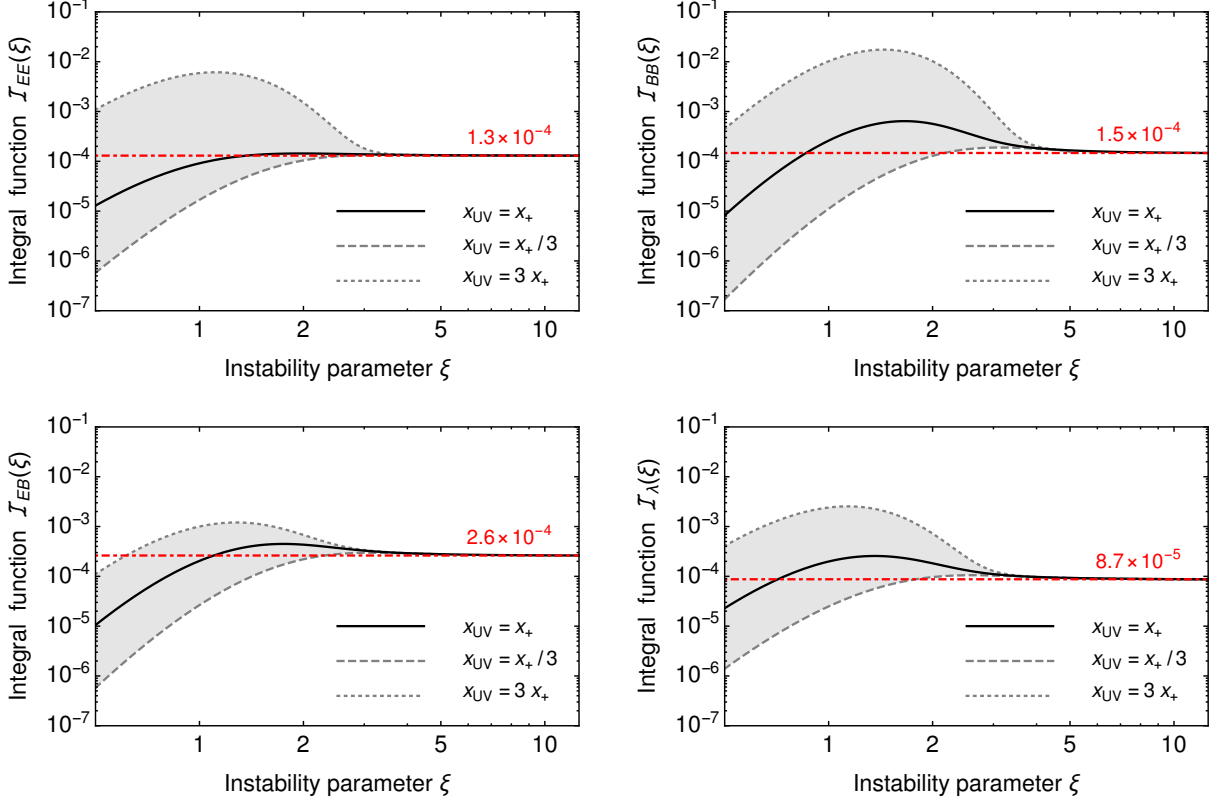


Figure 1: Dependence of the integral functions \mathcal{I}_{EE} (**upper left panel**), \mathcal{I}_{BB} (**upper right panel**), \mathcal{I}_{EB} (**lower left panel**), and \mathcal{I}_λ (**lower right panel**), on the instability parameter ξ ; see Eqs. (14), (20), and (28). For each function, we illustrate the effect of varying the UV cut-off scale (parametrized in terms of the upper integration boundary x_{UV}) within roughly one order of magnitude. At any given value of ξ , the parameter x_+ corresponds to $x_+ = 2\xi$; see Eq. (13). The red numbers and horizontal lines indicate the respective asymptotic values at $\xi \gg 1$.

terms in Eqs. (6) and (9). We are mainly interested in the following two ratios,

$$\delta_F = \frac{\rho_{EE} + \rho_{BB}}{3H^2 M_{\text{Pl}}^2}, \quad \delta_{\text{KG}} = \left| \frac{\rho_{EB}/\Lambda}{3H\dot{a}} \right| = \left| \frac{\rho_{EB}}{6\xi\Lambda^2 H^2} \right|. \quad (22)$$

Here, δ_F quantifies the hyper-EM contributions to the Friedmann equation, while δ_{KG} measures the importance of the source term in the Klein-Gordon equation in comparison to the Hubble friction term. For $4 \lesssim \xi \lesssim 10$, these two ratios are well fit by the following numerical expressions,

$$\delta_F \simeq 2.8 \times 10^{-4} \exp[0.90 \times 2\pi(\xi - 5)] \left(\frac{H}{10^{13} \text{ GeV}} \right)^2, \quad (23)$$

$$\delta_{\text{KG}} \simeq 7.6 \times 10^{-4} \exp[0.83 \times 2\pi(\xi - 5)] \left(\frac{H}{10^{13} \text{ GeV}} \right)^2 \left(\frac{3 \times 10^{17} \text{ GeV}}{\Lambda} \right)^2.$$

These relations are the first important results of our analysis. We stress that they represent numerical fit functions, which we obtain by fitting δ_F and δ_{KG} as functions of $e^{2\pi\xi}$, H^2 , and Λ^{-2} . The factors 0.90 and 0.83 in front of $2\pi\xi$ in Eq. (23) account for the competition between the exponentials ($e^{2\pi\xi}$) and the inverse powers (ξ^{-3} , ξ^{-4} , and ξ^{-5}) of ξ in Eq. (19). In Fig. 2, we compare our fit functions with the corresponding exact expressions for δ_F and δ_{KG} in Eq. (22).

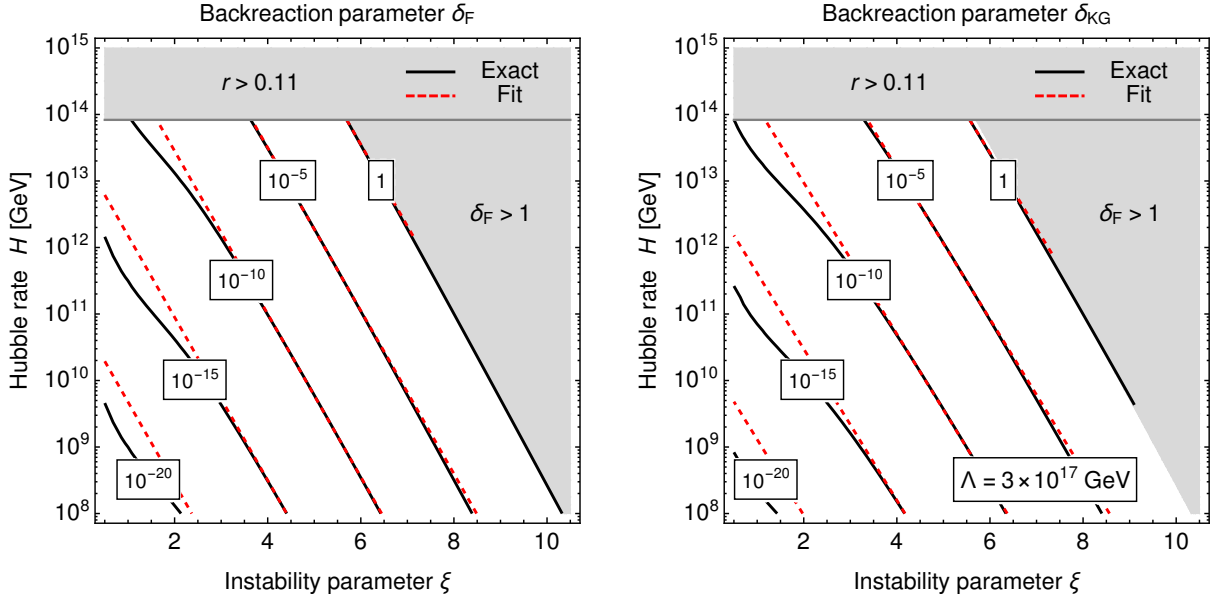


Figure 2: Backreaction parameters δ_F (**left panel**) and δ_{KG} (**right panel**) as functions of the instability parameter ξ and the Hubble rate H . The parameter δ_F quantifies the amount of backreaction in the Friedmann equation, while the parameter δ_{KG} quantifies the amount of backreaction in the Klein-Gordon equation; see Eq. (22). The black solid contours represent the exact expressions for δ_F and δ_{KG} , including the complicated ξ dependence of the integral functions in Eq. (20). The red dashed contours represent the numerical fit functions in Eq. (23). In the right panel, the suppression scale Λ is fixed at $\Lambda = 3 \times 10^{17} \text{ GeV}$. The scaling of δ_{KG} with Λ is trivial, $\delta_{KG} \propto \Lambda^{-2}$. By definition, values of δ_F larger than unity are unphysical; see Eq. (24). For values of the Hubble rate greater than $H \simeq 8 \times 10^{13} \text{ GeV}$, the PLANCK constraint on the tensor-to-scalar ratio, $r \lesssim 0.11$, is violated.

From Eq. (23), we see that the backreaction from the gauge field on the inflationary dynamics is negligible, at least for the chosen reference values. This conclusion drastically changes as soon as we go to larger values of ξ and H as well as to smaller values of Λ . Here, we find in particular an upper bound on ξ , such that the ratio δ_F does not take values larger than unity; see Fig. 2,

$$\delta_F \leq 1 \quad \Rightarrow \quad \xi \leq \xi_{\max}(H) \simeq 6.4 - 0.82 \log_{10} \left(\frac{H}{10^{13} \text{ GeV}} \right). \quad (24)$$

This bound is model-independent and needs to be obeyed by any model of pseudoscalar inflation coupled to an Abelian gauge sector. For ξ values beyond this bound, one formally finds that more than 100% of the total energy density is stored in the hyper-EM field. This signals that the backreaction from the excited gauge fields is no longer negligible in the Friedmann equation; and hence the above solutions are no longer trustable. Meanwhile, the ratio δ_{KG} can be varied independently, even if ξ satisfies Eq. (24), simply by adjusting the strength of the axion-gauge-field coupling. According to Eq. (23), lowering the suppression scale Λ by a factor 10 readily increases δ_{KG} by two orders of magnitude. For the same values of ξ and H as in Eq. (23), $\xi = 5$ and $H = 10^{13} \text{ GeV}$, but with $\Lambda = 3 \times 10^{16} \text{ GeV}$, the source term in Eq. (9) begins to compete with the Hubble friction term, $\delta_{KG} \sim 0.1$. As we will see in the following, such small values of Λ , however, turn out to be incompatible with the idea of baryogenesis from pseudoscalar inflation.

2.3 Hypermagnetic field at the end of inflation

As long as we stay sufficiently far away from the maximal ξ value in Eq. (24) and as long as the suppression scale Λ is not chosen too small, the effect of gauge field production merely represents a small (and most often completely negligible) perturbation of the inflationary dynamics. In this regime, we can therefore safely trust our analysis in the previous section. In particular, we can use our result for the hypermagnetic field energy density, ρ_{BB} , in Eq. (19) to estimate the physical hypermagnetic field strength, B_p , at any given time during inflation,

$$B_p^2 = 2\rho_{BB} = \langle \mathbf{B}^2 \rangle = \frac{1}{R^4} \int \frac{d^3\mathbf{k}}{(2\pi)^3} k^2 |A_+^k|^2 = 2 \mathcal{I}_{BB}(\xi) \frac{e^{2\pi\xi}}{\xi^5} H^4, \quad (25)$$

where we again neglect the vacuum contributions from the negative-helicity modes. This field strength is the evident manifestation of *primordial magnetogenesis* in models of pseudoscalar inflation coupled to the hypercharge gauge field. For typical values of ξ and H , one finds

$$B_p \simeq 1.1 \times 10^{49} \text{ G} \left(\frac{f_{BB}(\xi)}{f_{BB}(5)} \right)^{1/2} \left(\frac{H}{10^{13} \text{ GeV}} \right)^2, \quad f_{BB}(\xi) = \mathcal{I}_{BB}(\xi) \frac{e^{2\pi\xi}}{\xi^5}. \quad (26)$$

In the next section, we will discuss the postinflationary evolution of this primordial hypermagnetic field, arguing that it is not completely erased during the radiation-dominated era. The primordial hypermagnetic field may, in fact, survive all the way up to the present epoch and contribute to the intergalactic magnetic fields that we observe today.

Another important quantity that characterizes the primordial hypermagnetic field is the physical correlation length, λ_p . To estimate λ_p , we compute the average of all relevant wavelengths, weighted by their respective contributions to the energy density ρ_{BB} ,

$$\lambda_p = \frac{1}{\rho_{BB}} \frac{1}{2R^4} \int \frac{d^3\mathbf{k}}{(2\pi)^3} \frac{2\pi R}{k} k^2 |A_+^k|^2 = \xi \frac{\mathcal{I}_\lambda(\xi)}{\mathcal{I}_{BB}(\xi)} \frac{2\pi}{H}. \quad (27)$$

Here, the integral function \mathcal{I}_λ is defined in analogy to the three functions in Eq. (20)

$$\mathcal{I}_\lambda(\xi) = \frac{\xi^4}{8\pi^2} e^{-\pi\xi} \int_0^{x_{UV}} dx x^2 |W_{\kappa_+, 1/2}(-2ix)|^2. \quad (28)$$

Similarly as the other integral functions, \mathcal{I}_λ becomes insensitive to the exact choice of x_{UV} as soon as it approaches its asymptotic value. For $\xi \gtrsim 4$, it is well approximated by $\mathcal{I}_\lambda \simeq 8.7 \times 10^{-5}$; see Fig. 1. Together with the asymptotic value for \mathcal{I}_{BB} , this shows that the hypermagnetic fields typically exhibit a correlation length that extends over more than one Hubble radius,

$$\lambda_p \simeq 3.0 \left(\frac{\xi}{5} \right) \lambda_H, \quad \lambda_H = \frac{2\pi}{H}. \quad (29)$$

More explicitly, we find that λ_p typically takes values of the following order of magnitude,

$$\lambda_p \simeq 1.1 \times 10^{-50} \text{ Mpc} \left(\frac{f_\lambda(\xi)}{f_\lambda(5)} \right) \left(\frac{10^{13} \text{ GeV}}{H} \right), \quad f_\lambda(\xi) = \xi \frac{\mathcal{I}_\lambda(\xi)}{\mathcal{I}_{BB}(\xi)}. \quad (30)$$

The above expressions for B_p and λ_p in Eqs. (25) and (27) are valid at any time during inflation. In the following, we are however going to be mostly interested in the values of B_p

and λ_p at the end of inflation, i.e., at the onset of reheating. In this paper, we will work in the approximation of instant reheating, such that the end of inflation coincides with the beginning of the radiation-dominated era. To find the values of B_p and λ_p at this time, it is, therefore, sufficient to simply evaluate Eqs. (25) and (27) for $H = H_{\text{rh}}$ and $\xi = \xi_{\text{rh}}$, where H_{rh} and ξ_{rh} respectively denote the Hubble rate and the instability parameter at the end of inflation. Both quantities are model-dependent, which is why we will treat them as free parameters in the following. At this point it is interesting to note that, for most models of interest, ξ_{rh} is entirely controlled by the strength of the axion-gauge-field coupling. To see this, let us suppose that the end of inflation is triggered by a violation of the first slow-roll condition. That is, inflation ends because the Hubble parameter H is no longer quasi-constant. This condition is conveniently quantified in terms of the slow-roll parameter ε . Let us assume for now that the backreaction from gauge field production is negligible. In the usual slow-roll approximation, one then has

$$\varepsilon = \frac{d \ln H}{dN_e} \approx \frac{M_{\text{Pl}}^2}{2} \left(\frac{d \ln V}{da} \right)^2 \approx \frac{\dot{a}^2}{2H^2 M_{\text{Pl}}^2}, \quad (31)$$

where N_e denotes the number of e-folds until the end of inflation. Next, let us rewrite the condition $\varepsilon \sim 1$ at the end of inflation in terms of ξ_{rh} and Λ . This yields

$$\varepsilon \approx \frac{2\xi_{\text{rh}}^2 \Lambda^2}{M_{\text{Pl}}^2} \sim 1 \quad \Rightarrow \quad \xi_{\text{rh}} \sim \frac{M_{\text{Pl}}}{\sqrt{2}\Lambda} \simeq 5.7 \left(\frac{3 \times 10^{17} \text{ GeV}}{\Lambda} \right). \quad (32)$$

Together with Eq. (23), this result confirms that, for $\Lambda \gtrsim 3 \times 10^{17} \text{ GeV}$, the backreaction on the inflationary dynamics is mostly negligible at all times. For smaller values of Λ , the ratio δ_{KG} however quickly approaches values of order unity towards the end of inflation.

3 Gauge field evolution after inflation

We now turn to the description of the postinflationary evolution of the primordial gauge fields. We will discuss in turn the different stages until the beginning of the inverse cascade regime (see Sec. 3.1), until the electroweak phase transition (see Sec. 3.2), and until today (see Sec. 3.3).

3.1 From the end of inflation to the onset of the inverse cascade regime

As stressed several times before, we are going to work in the approximation of instant reheating.⁸ That is, we make the simplifying assumption that, at the end of inflation, the vacuum energy density driving inflation is converted instantaneously into thermal radiation,

$$\rho_{\text{inf}}(t_{\text{rh}}) = 3H_{\text{rh}}^2 M_{\text{Pl}}^2 \quad \rightarrow \quad \rho_{\text{rad}}(t_{\text{rh}}) = \frac{\pi^2}{30} g_* T_{\text{rh}}^4, \quad (33)$$

⁸Similarly, we also assume that there is no charged plasma even as a subdominant component of the universe until the end of inflation. The presence of such a charged plasma component already during the stage of inflation might prevent the hypermagnetic helicity from developing and, hence, change our estimate.

where $g_* = 106.75$ denotes the effective number of relativistic DOFs in the standard model. We consequently neglect the period of inflaton oscillations after inflation as well as the gradual production of (charged) particles in inflaton decays. This assumption simplifies our analysis considerably—given the fact that the charged particles in the emerging plasma actually interfere with the evolution of the primordial gauge fields.⁹ A reliable description of this complicated process however requires a dedicated numerical simulation that takes into account both nonperturbative particle production and MHD, which is not yet available and which is certainly beyond the scope of this work. The assumption of instant reheating moreover allows us to eliminate the reheating temperature T_{rh} as a free parameter in our scenario. According to Eq. (33), we can simply express T_{rh} in terms of the Hubble rate at the end of inflation, H_{rh} ,

$$T_{\text{rh}} = \sqrt{M_* H_{\text{rh}}} \simeq 2.7 \times 10^{15} \text{ GeV} \left(\frac{H_{\text{rh}}}{10^{13} \text{ GeV}} \right)^{1/2}, \quad M_* = \left(\frac{90}{\pi^2 g_*} \right)^{1/2} M_{\text{Pl}}. \quad (34)$$

By employing this relation, we choose to discard all details of the reheating process. While this introduces an uncertainty to some degree, it also makes our analysis more model-independent.

To describe the behavior of the primordial gauge fields after reheating, we shall follow the discussion in [47, 71, 73] (see also [46, 55, 68]). Our first observation is that, once the plasma is in place, the hyper-EM field begins to interact with hypercharged particles in the thermal bath. This interaction makes the primordial hyperelectric fields vanishingly small, $\mathbf{E} \simeq 0$ (i.e., \mathbf{E} becomes suppressed by the large electric conductivity), leaving us mainly with the hypermagnetic \mathbf{B} field. In the following, we will assume that, initially, the backreaction from the charged particles has neither an impact on the overall strength of the hypermagnetic field, B_p , nor on its correlation length, λ_p . The starting point of our analysis are, therefore, our results for B_p and λ_p that we obtained in Sec. 2.3; see Eqs. (25) and (27),

$$B_p^{\text{rh}} = (2\mathcal{I}_{BB})^{1/2} \frac{e^{\pi\xi_{\text{rh}}}}{\xi_{\text{rh}}^{5/2}} H_{\text{rh}}^2 \simeq 1.7 \times 10^{-2} \frac{e^{\pi\xi_{\text{rh}}}}{\xi_{\text{rh}}^{5/2}} H_{\text{rh}}^2, \quad \lambda_p^{\text{rh}} = \xi_{\text{rh}} \frac{\mathcal{I}_\lambda}{\mathcal{I}_{BB}} \frac{2\pi}{H_{\text{rh}}} \simeq 3.7 \frac{\xi_{\text{rh}}}{H_{\text{rh}}}. \quad (35)$$

We are now going to outline how these two quantities behave as functions of the radiation temperature T , as the universe expands. Our final results are summarized schematically in Fig. 3, which illustrates the time dependence of B_p and λ_p for different values of ξ_{rh} and H_{rh} .

At early times, i.e., directly after reheating, we expect that both the field strength B_p as well as the correlation length λ_p simply redshift adiabatically [62],

$$B_p(T) = \left(\frac{R_{\text{rh}}}{R(T)} \right)^2 B_p^{\text{rh}}, \quad \lambda_p(T) = \left(\frac{R(T)}{R_{\text{rh}}} \right) \lambda_p^{\text{rh}}. \quad (36)$$

This expectation is justified by the fact that, initially, the correlation length λ_p is much longer than the eddy scale of the velocity fields of the charged plasma, $\lambda_T \simeq vt$, (see also the discussion in the next section) implying that the charged plasma cannot affect the evolution of the hypermagnetic field. During radiation domination and for a constant number of effective DOFs, the

⁹The oscillations of the inflaton field would enhance the production of primordial gauge fields [76]. But, at the same time, the high electric conductivity of the charged plasma would suppress the hypermagnetic helicity [78].

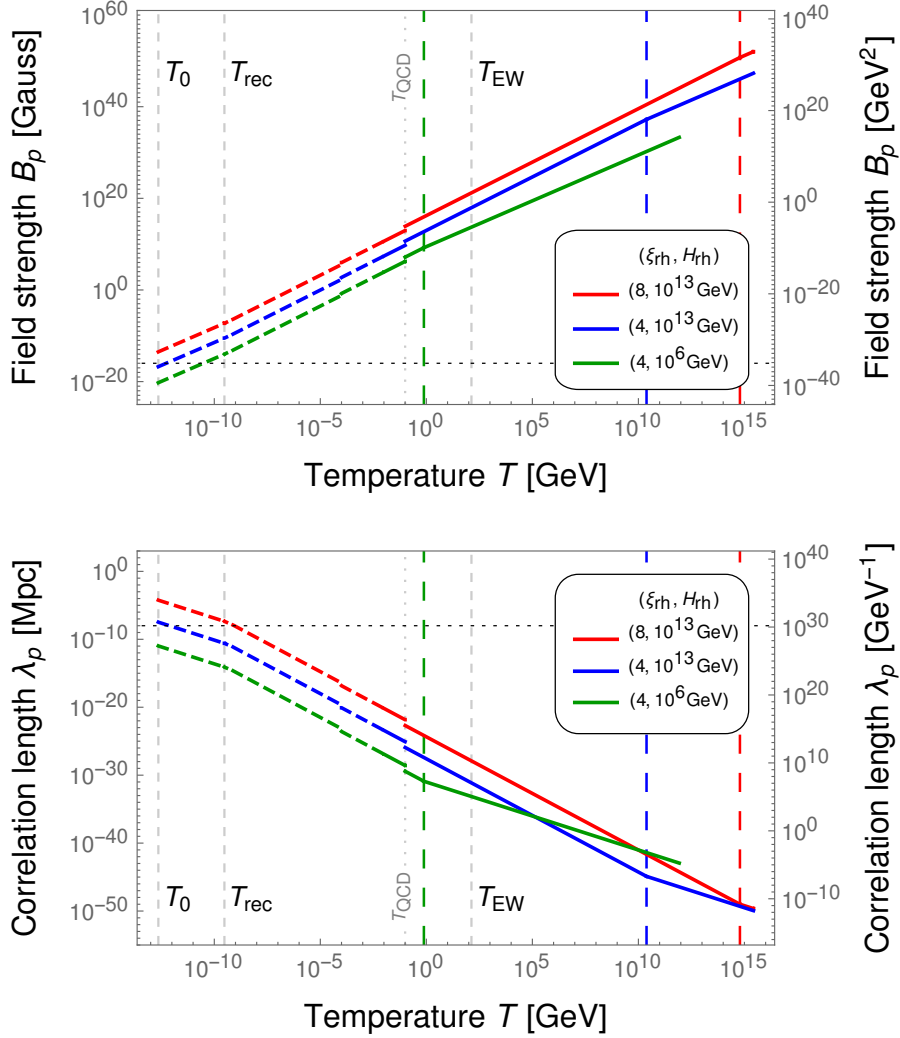


Figure 3: Physical field strength B_p (**upper panel**) and physical correlation length λ_p (**lower panel**) of the hypermagnetic \mathbf{B} field as functions of the radiation temperature T for representative values of H and ξ at the end of inflation. The vertical dotted lines mark the respective temperatures at which the adiabatic regime transitions into the inverse cascade regime. Both plots account for the decrease in the effective number of DOFs in the course of the expansion. The kinks around $T \sim 100$ MeV correspond, e.g., to the QCD phase transition. For $T < 10$ MeV, damping effects might become important (see [47, 71, 73]) and our description of the magnetic field evolution becomes less accurate. For this reason, we only draw dashed lines in the low-temperature regime.

scale factor R increases in inverse proportion to the plasma temperature, $R \propto 1/T$. During the early phase of adiabatic expansion, B_p therefore drops like T^2 , while λ_p grows like $1/T$.

3.2 From the onset of the inverse cascade regime to the electroweak crossover

In the course of the further evolution, the interaction of the \mathbf{B} field and the charged plasma (described by the velocity field \mathbf{v}) results in a complicated co-evolution of both fields, governed by the MHD equations: The \mathbf{B} field induces a \mathbf{v} field and the \mathbf{v} field back-reacts on the evolution of the \mathbf{B} field, which likely results in turbulent field configurations. If the charged plasma develops a turbulence, the scale up to which the velocity field is capable of affecting the \mathbf{B} field can be estimated in terms of the turbulence (or eddy) scale λ_T ,

$$\lambda_T \simeq vt = \frac{v}{2H}, \quad v = |\mathbf{v}|. \quad (37)$$

As long as $\lambda_T \ll \lambda_p$, the \mathbf{v} field affects the \mathbf{B} field only on small scales and the evolution of B_p and λ_p remains unaffected. Both the turbulence scale λ_T and the correlation length λ_p grow with time. However, λ_T grows faster than λ_p , such that, after some finite time, the turbulence scale catches up with the correlation length, $\lambda_T \sim \lambda_p$. After that, the \mathbf{B} field can no longer evolve adiabatically. Indeed, it has been observed in MHD simulations that a maximally helical magnetic field generates a turbulent plasma and that the kinetic energy of the plasma waves becomes comparable to (or equilibrated with) the energy stored in the hypermagnetic field [71, 73], $\rho_{\text{kin}} \sim \rho_{BB}$. This means that the amplitude of the \mathbf{v} field is comparable to the Alfvén velocity v_A . In the nonrelativistic limit, $v_A \ll 1$, the Alfvén velocity is given as [81],

$$v \sim v_A = \frac{v_A^0}{\sqrt{1 + (v_A^0)^2}} \sim v_A^0, \quad v_A^0 = \frac{B_p}{\sqrt{\rho_{\text{ch}} + p_{\text{ch}}}}, \quad \rho_{\text{ch}} = \frac{\pi^2}{30} g_{*,\text{ch}} T^4, \quad p_{\text{ch}} = \frac{\rho_{\text{ch}}}{3}, \quad (38)$$

with ρ_{ch} and p_{ch} denoting the energy density and pressure of the hypercharged particles in the plasma. $g_{*,\text{ch}} = 82.75$ counts the effective number of relativistic DOFs carrying nonzero hypercharge in the standard model. In the following, we will not distinguish between v_A and v_A^0 and simply approximate $v_A \approx v_A^0$. Combining Eqs. (37) and (38) and assuming that the \mathbf{B} and \mathbf{v} fields are equilibrated even in the adiabatic regime, we find for λ_T in the adiabatic regime

$$\lambda_T \propto \frac{B_p}{\sqrt{\rho_{\text{ch}}} H} \propto R^2 \propto \frac{1}{T^2} \quad (39)$$

Indeed, this corresponds to a faster growth than in the case of λ_p , which simply scales like $1/T$.

Once the turbulence scale has caught up with the correlation length, $\lambda_T \sim \lambda_p$, the hypermagnetic field enters into the inverse cascade regime [69–71]. From this point on, the growth of λ_p is simply driven by the turbulence scale λ_T , such that $\lambda_T \sim \lambda_p$ at all subsequent times,

$$\lambda_p \sim \lambda_T \propto \frac{B_p}{\sqrt{\rho_{\text{ch}}} H} \quad \Rightarrow \quad \frac{\lambda_p}{B_p} \propto \frac{1}{\sqrt{\rho_{\text{ch}}} H} \propto R^4 \propto \frac{1}{T^4}. \quad (40)$$

This relation is, however, not yet sufficient to fully estimate the scaling behavior of B_p and λ_p during the inverse cascade regime. In addition to Eq. (40), we need a second, independent relation between λ_T and B_p . At this point, it comes in handy that, as a consequence of the high hyperelectric conductivity of the charged plasma, the comoving helicity density h_c is approximately conserved at high temperatures; see, e.g., [61, 62] and references therein,¹⁰

$$h_c = \lim_{V \rightarrow \infty} \frac{1}{V} \int_V d^3\mathbf{x} \mathbf{A}_c \cdot \mathbf{B}_c \sim \text{const}. \quad (41)$$

Here, the integral over the volume V represents nothing but a spatial average, $h_c = \langle \mathbf{A}_c \mathbf{B}_c \rangle$. Moreover, we emphasize that both vector fields, $\mathbf{A}_c \equiv \mathbf{A}$ and $\mathbf{B}_c = R^2 \mathbf{B}$, correspond to comoving quantities. We roughly estimate the typical size of \mathbf{A}_c as $A_c \sim \lambda_c / (2\pi) B_c \propto R \lambda_p B_p$, such that

$$h_c = R^2 \langle \mathbf{A} \mathbf{B} \rangle \propto R^3 \lambda_p B_p^2 \sim \text{const}. \quad (42)$$

Together with Eq. (40), this relation then yields the scaling behavior of B_p and λ_p ,

$$B_p \propto \frac{1}{R^{7/3}} \propto T^{7/3}, \quad \lambda_p \propto R^{5/3} \propto \frac{1}{T^{5/3}}, \quad (43)$$

which coincides with the scaling laws of the inverse cascade found in MHD simulations [71, 73].

We stress that all of the relations in Eqs. (37), (38), (40), and (42) are simply rough estimates. A more careful treatment would require a full-fledged MHD simulation [47, 68], which is beyond the scope of this work. Moreover, the study of primordial magnetic fields in MHD simulations is still the subject of on-going work in the literature. In anticipation of new simulations, we shall therefore settle for the estimates above, leaving any refinement of our analysis for future work.

Next, let us determine the temperature at the onset of the inverse cascade regime. We find the transition temperature, $T = T_{\text{ic}}$, simply by solving the condition $\lambda_T(T_{\text{ic}}) = \lambda_p(T_{\text{ic}})$ for T_{ic} ,

$$\frac{T_{\text{ic}}}{T_{\text{rh}}} = \frac{\mathcal{I}_{BB}^{3/2}}{4\sqrt{2}\pi\mathcal{I}_\lambda} \left(\frac{g_*}{g_{*,\text{ch}}} \right)^{1/2} \frac{e^{\pi\xi_{\text{rh}}} H_{\text{rh}}}{\xi_{\text{rh}}^{7/2} M_{\text{Pl}}} \simeq 1.3 \times 10^{-3} \frac{e^{\pi\xi_{\text{rh}}} H_{\text{rh}}}{\xi_{\text{rh}}^{7/2} M_{\text{Pl}}}, \quad (44)$$

where we used that $T_{\text{rh}} = \sqrt{M_* H_{\text{rh}}}$. The Alfvén velocity v_A at this temperature is given as

$$v_A = \frac{\mathcal{I}_{BB}^{1/2}}{\sqrt{2}} \left(\frac{g_*}{g_{*,\text{ch}}} \right)^{1/2} \frac{e^{\pi\xi_{\text{rh}}} H_{\text{rh}}}{\xi_{\text{rh}}^{5/2} M_{\text{Pl}}} \simeq 9.7 \times 10^{-3} \frac{e^{\pi\xi_{\text{rh}}} H_{\text{rh}}}{\xi_{\text{rh}}^{5/2} M_{\text{Pl}}}, \quad (45)$$

Furthermore, we are now in the position to calculate the field strength as well as the correlation length of the hypermagnetic field at $T = T_{\text{ic}}$. Combining Eqs. (35), (36), and (44), we obtain

$$B_p^{\text{ic}} = \left(\frac{T_{\text{ic}}}{T_{\text{rh}}} \right)^2 B_p^{\text{rh}} = \frac{\mathcal{I}_{BB}^{7/2}}{16\sqrt{2}\pi^2\mathcal{I}_\lambda^2} \frac{g_*}{g_{*,\text{ch}}} \frac{e^{3\pi\xi_{\text{rh}}} H_{\text{rh}}^4}{\xi_{\text{rh}}^{19/2} M_{\text{Pl}}^2} \simeq 2.9 \times 10^{-8} \frac{e^{3\pi\xi_{\text{rh}}} H_{\text{rh}}^4}{\xi_{\text{rh}}^{19/2} M_{\text{Pl}}^2}, \quad (46)$$

$$\lambda_p^{\text{ic}} = \left(\frac{T_{\text{rh}}}{T_{\text{ic}}} \right) \lambda_p^{\text{rh}} = \frac{8\sqrt{2}\pi^2\mathcal{I}_\lambda^2}{\mathcal{I}_{BB}^{5/2}} \left(\frac{g_{*,\text{ch}}}{g_*} \right)^{1/2} \frac{\xi_{\text{rh}}^{9/2} M_{\text{Pl}}}{e^{\pi\xi_{\text{rh}}} H_{\text{rh}}^2} \simeq 2.9 \times 10^3 \frac{\xi_{\text{rh}}^{9/2} M_{\text{Pl}}}{e^{\pi\xi_{\text{rh}}} H_{\text{rh}}^2}.$$

¹⁰Based on Ampère's and Ohm's laws, one can show that the time derivative of h_c is suppressed by the inverse of the hyperelectric conductivity, $\dot{h}_c \propto 1/\sigma$. The fact that h_c is conserved to good approximation is, therefore, a direct consequence of the large (but finite) conductivity of the standard model plasma, $\sigma \sim 10^2 T$ [82, 83].

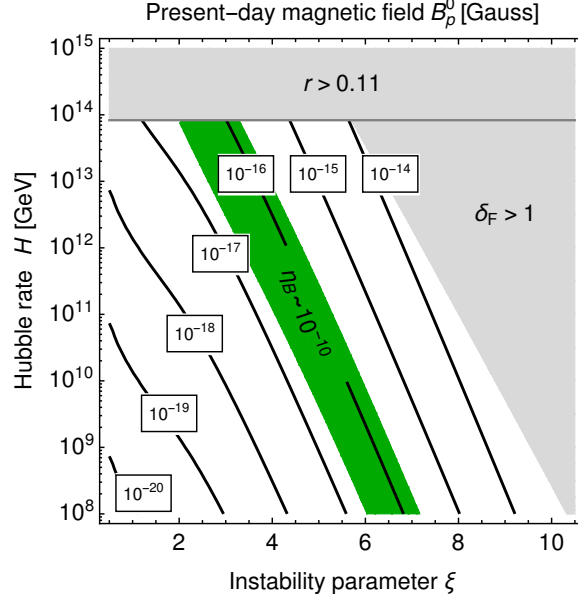


Figure 4: Present-day strength of the physical magnetic field, B_p^0 , as a function of the instability parameter ξ and the Hubble rate H ; see Eq. (50). Here, both ξ and H are understood to correspond to the respective values at the end of inflation, $\xi \equiv \xi_{\text{rh}}$ and $H \equiv H_{\text{rh}}$. The green band illustrates the region in parameter space where baryogenesis around the time of EWSB results in a baryon asymmetry η_B in accord with the observed value, $\eta_B^{\text{obs}} \sim 10^{-10}$; see Eq. (62) and Fig. 5. The gray-shaded regions are the same as in Fig. 2.

At temperatures below T_{ic} , the field strength B_p behaves as follows; see Eq. (43),

$$\begin{aligned}
 B_p(T) &= \left(\frac{T}{T_{\text{ic}}}\right)^{7/3} B_p^{\text{ic}} = \left(\frac{T}{T_{\text{rh}}}\right)^{7/3} \left[16 \pi \mathcal{I}_\lambda \left(\frac{g_{*,\text{ch}}}{g_*}\right)^{1/2} \frac{e^{2\pi\xi_{\text{rh}}}}{\xi_{\text{rh}}^4} H_{\text{rh}}^5 M_{\text{Pl}} \right]^{1/3} \\
 &\simeq 0.16 \left(\frac{T}{T_{\text{rh}}}\right)^{7/3} \left(\frac{e^{2\pi\xi_{\text{rh}}}}{\xi_{\text{rh}}^4} H_{\text{rh}}^5 M_{\text{Pl}}\right)^{1/3},
 \end{aligned} \tag{47}$$

whereas for the correlation length λ_p , we find

$$\begin{aligned}
 \lambda_p(T) &= \left(\frac{T_{\text{ic}}}{T}\right)^{5/3} \lambda_p^{\text{ic}} = \left(\frac{T_{\text{rh}}}{T}\right)^{5/3} \left(\frac{\pi \mathcal{I}_\lambda}{4} \frac{g_*}{g_{*,\text{ch}}} \frac{e^{2\pi\xi_{\text{rh}}}}{\xi_{\text{rh}}^4} \frac{1}{H_{\text{rh}} M_{\text{Pl}}^2}\right)^{1/3} \\
 &\simeq 4.5 \times 10^{-2} \left(\frac{T_{\text{rh}}}{T}\right)^{5/3} \left(\frac{e^{2\pi\xi_{\text{rh}}}}{\xi_{\text{rh}}^4} \frac{1}{H_{\text{rh}} M_{\text{Pl}}^2}\right)^{1/3}.
 \end{aligned} \tag{48}$$

Note that we assumed a constant effective number of DOFs in both Eq. (47) and Eq. (48).

3.3 From the electroweak crossover to the present epoch

The evolution of the field strength and correlation length at late times can be described by standard techniques with the assumption that the magnetic fields evolve according to the inverse cascade until recombination and evolve adiabatically again after that until today. In the usual Λ CDM model (without any additional stages of late-time entropy production or the like), we can readily relate the values of B_p and λ_p around the time of EWSB to their values in the present

epoch,

$$B_p^0 \simeq 1.1 \times 10^{-14} \text{ G} \left(\frac{B_p^{\text{ew}}}{10^{20} \text{ G}} \right) \left(\frac{100 \text{ GeV}}{T_{\text{ew}}} \right)^{7/3}, \quad (49)$$

$$\lambda_p^0 \simeq 0.40 \text{ pc} \left(\frac{\lambda_p^{\text{ew}}}{10^{-29} \text{ Mpc}} \right) \left(\frac{T_{\text{ew}}}{100 \text{ GeV}} \right)^{5/3},$$

which is consistent with the corresponding relations in [62, 63]. Here, the values of B_p^{ew} and λ_p^{ew} simply follow from evaluating our results in Eq. (47) and Eq. (48) at $T = T_{\text{ew}} \sim 100 \text{ GeV}$, i.e., the temperature at the time of EWSB.¹¹ We then obtain the following final expression for the present-day strength of the physical magnetic field,

$$B_p^0 \simeq 6.0 \times 10^{-18} \text{ G} \left[\mathcal{I}_\lambda \left(\frac{g_{*,\text{ch}}}{g_*} \right)^{1/2} \frac{e^{2\pi\xi_{\text{rh}}}}{\xi_{\text{rh}}^4} \right]^{1/3} \left(\frac{H_{\text{rh}}}{10^{13} \text{ GeV}} \right)^{1/2} \quad (50)$$

$$\simeq 2.5 \times 10^{-19} \text{ G} \left(\frac{e^{2\pi\xi_{\text{rh}}}}{\xi_{\text{rh}}^4} \right)^{1/3} \left(\frac{H_{\text{rh}}}{10^{13} \text{ GeV}} \right)^{1/2},$$

which we plot as a function of ξ_{rh} and H_{rh} in Fig. 4. This relation illustrates how the explosive production of gauge fields during pseudoscalar inflation results in magnetic fields on astrophysical scales in the present epoch. Note that B_p^0 in Eq. (50) does not depend on the exact value of T_{ew} . Moreover, it only depends on \mathcal{I}_λ and is independent of the integral function \mathcal{I}_{BB} . Meanwhile, we find that the present-day value of the correlation length, λ_p^0 , satisfies exactly the relation which one expects for causally generated magnetic fields [73]; see also Eq. (4) and footnote 5,

$$\lambda_p^0 \simeq 0.28 \text{ pc} \left(\frac{B_p^0}{10^{-14} \text{ G}} \right) \simeq \frac{1.0 \text{ pc}}{(4\pi)^{1/2}} \left(\frac{B_p^0}{10^{-14} \text{ G}} \right). \quad (51)$$

We stress that this result is based on the strict relation $v = v_A$; see Eq. (38). However, there are also MHD simulations suggesting that v might in fact be slightly suppressed compared to the Alfvén velocity, $v \simeq \mathcal{O}(0.1) v_A$ [71, 73]. Thus, our above estimates come with at least an $\mathcal{O}(10)$ uncertainty.¹² Nonetheless, we expect our expressions to catch the basic *qualitative* features of the magnetic field from pseudoscalar inflation, in particular, the relation between the inflationary parameters H and ξ on the one hand and the quantities B_p and λ_p on the other hand.

4 Implications for baryon asymmetry and gravitational waves

The primordial gauge fields generated during inflation have important phenomenological consequences. Not only do they seed the intergalactic magnetic fields that permeate our Universe today (see Eq. (50)), they also lead to the generation of a nonzero baryon number around the time of EWSB (see Sec. 4.1) as well as to a signal in the stochastic GW background at high frequencies (see Sec. 4.2). We shall now discuss these two phenomena in turn.

¹¹During EWSB, the hypermagnetic \mathbf{B}_Y field turns into the electromagnetic \mathbf{B}_{EM} field. The amplitudes $|\mathbf{B}_Y|$ and $|\mathbf{B}_{\text{EM}}|$ are, however, continuously connected [64], which is why we do not distinguish between them here.

¹²Note that we also omitted possible damping effects at low temperatures, $T < 10 \text{ MeV}$, due to processes such as neutrino and photon free streaming. However, despite these effects, it has been demonstrated that both the field strength and the correlation length eventually reach the same values as in the simple inverse-cascade estimate [73].

4.1 Baryogenesis from pseudoscalar inflation

The gauge fields generated during inflation are maximally helical. This can be seen explicitly from our analysis in Sec. 2.1, where we showed that only modes in one helicity eigenstate are exponentially amplified during inflation, while the other helicity modes stay at the vacuum level; see Eq. (17). Moreover, we found that the sign of the final helicity depends on the sign of the inflaton velocity, $\text{sgn } \mathcal{H} = \text{sgn } \dot{a}$. In Sec. 2.1, we chose $\dot{a} > 0$, in order to achieve positive helicity.

Changes in the comoving helicity density h_c (see Eq. (41)) after inflation are suppressed by the hyperelectric conductivity of the thermal plasma, $\dot{h}_c \propto 1/\sigma$; see footnote 10. Therefore, given the large value of σ in the standard model, $\sigma \sim 10^2 T$ [82, 83], h_c is *approximately* conserved after inflation; see Eq. (42). At the same time, it is important to remember that any change in the hypermagnetic helicity results in the production of baryon number B and lepton number L . This is reflected in Eq. (3), which follows from the chiral triangle anomaly in the standard model. Therefore, even slight changes in h_c , because of the finite conductivity σ , are physically relevant as soon as we turn our attention to the time evolution of B and L . This observation is the basis for the scenario of *baryogenesis via decaying hypermagnetic helicity* [61–65]. In the following, we will illustrate how this scenario fits together with our analysis of primordial magnetogenesis in models of pseudoscalar inflation. In doing so, we will follow the discussion in [64] (see also [63]).

In analogy to h_c in Eq. (41), we may define the physical helicity density h_p as follows,

$$h_p = \frac{h_c}{R^3} = \lim_{V \rightarrow \infty} \frac{1}{V} \int_V d^3 \mathbf{x} \mathbf{A}_p \cdot \mathbf{B}_p = \langle \mathbf{A}_p \mathbf{B}_p \rangle. \quad (52)$$

Here and only here, \mathbf{A}_p is defined as $\mathbf{A}_p = \mathbf{A}/R$, whereas $\mathbf{B}_p \equiv \mathbf{B}$ is nothing but the ordinary physical hypermagnetic \mathbf{B} field. Again, the angle brackets in Eq. (52) denote the volume average of the scalar product $\mathbf{A}_p \mathbf{B}_p$. One can show that the time derivative of the helicity density h_p is related to the (Abelian) Chern-Simons density of the hypercharge gauge field,

$$\frac{d}{dt} h_p = \frac{1}{2} \langle F_{\mu\nu} \tilde{F}^{\mu\nu} \rangle = -2 \langle \mathbf{E} \mathbf{B} \rangle. \quad (53)$$

According to the standard model chiral anomaly, the Chern-Simons density $F_{\mu\nu} \tilde{F}^{\mu\nu}$ contributes in turn to the divergence of the baryon and lepton number currents J_B^μ and J_L^μ ,

$$\partial_\mu J_B^\mu = \partial_\mu J_L^\mu = N_g \left(\frac{g_W^2}{16\pi^2} W_{\mu\nu}^a \tilde{W}_a^{\mu\nu} - \frac{g_Y^2}{32\pi^2} F_{\mu\nu} \tilde{F}^{\mu\nu} \right). \quad (54)$$

In combination with Eq. (53), the time integral of this equation results in the relation in Eq. (3).

For our purposes, the important conclusion from Eq. (3) is that a decaying hypermagnetic helicity, $\dot{h}_p \neq 0$, induces nonzero baryon and lepton number. To properly track the evolution of baryon number B as a function of time during this process, one needs to solve a coupled system of kinetic equations, which take into account all relevant effects; see [63, 64] for details. As it turns out, B is fixed after EWSB, i.e., at $T \sim 100$ GeV, since after EWSB, baryon and lepton number are no longer anomalously violated. In the kinetic equations, the generation

of baryon number because of the time-dependent hypermagnetic helicity is characterized by a temperature-dependent source term, $S = f\mathcal{S}$, which factorizes into two contributions,

$$f(\theta_W, T) = -T \frac{d\theta_W}{dT} \sin(2\theta_W), \quad \mathcal{S}(T) = \frac{H}{sT} \frac{h_p}{8\pi^2}. \quad (55)$$

Similarly as in the case of h_c (see Eq. (42)), we can estimate the magnitude of h_p as follows,

$$h_p \sim \frac{\lambda_p}{2\pi} B_p^2 \quad \Rightarrow \quad \mathcal{S} \sim \frac{H}{sT} \frac{\lambda_p B_p^2}{16\pi^3}, \quad (56)$$

where λ_p and B_p at $T \sim 100$ GeV are given in Eqs. (47) and (48).¹³ Note that \mathcal{S} is proportional to the amplitude of the hypermagnetic helicity, h_p . Meanwhile, f is a function of the weak mixing angle θ_W , which varies as a function of temperature during the electroweak crossover. For $d\theta_W/dT = 0$, the hypermagnetic helicity does not decay and hence the source S vanishes.

The production of baryon number because of the change in the weak mixing angle has to compete with the usual washout processes because of electroweak sphalerons. The effect of sphaleron washout is conveniently accounted for in the kinetic equations by a transport coefficient $\gamma_{w,\text{sph}}$. For a Higgs mass of 125 GeV, lattice simulations of the electroweak crossover yield [84],

$$\gamma_{w,\text{sph}} \simeq \exp \left[-147.7 + 107.9 \left(\frac{T}{130 \text{ GeV}} \right) \right], \quad \text{for } T \lesssim 161 \text{ GeV}, \quad (57)$$

where $T \simeq 130$ GeV is just the temperature at which the electroweak sphalerons freeze out. The resulting kinetic equations are quite complicated and need to be solved numerically. However, as shown in [64], the final baryon asymmetry is nicely reproduced by the following compact analytical expression,

$$\eta_B = \frac{n_B}{s} \simeq \frac{17}{37} \left[(g_W^2 + g_Y^2) \frac{f(\theta_W, T) \mathcal{S}}{\gamma_{w,\text{sph}}} \right]_{T=T_{\text{BAU}}}, \quad T_{\text{BAU}} = 135 \text{ GeV}. \quad (58)$$

Here, the baryogenesis temperature T_{BAU} is chosen, so as to optimize the agreement between the analytical result and the outcome of the numerical calculation.

Combining Eqs. (47), (48), (56), (57), and (58) and using $g_W \simeq 0.64$ and $g_Y \simeq 0.35$ at the electroweak scale, we obtain the following expression for the final baryon asymmetry,

$$\eta_B \simeq 2.9 \times 10^{-3} \mathcal{I}_\lambda \left[\frac{f(\theta_W, T)}{\gamma_{w,\text{sph}}} \left(\frac{e^{2\pi\xi_{\text{rh}}}}{\xi_{\text{rh}}^4} \right) \left(\frac{H_{\text{rh}}^3 T^2}{M_{\text{Pl}}^5} \right)^{1/2} \right]_{T=T_{\text{BAU}}}. \quad (59)$$

A reliable determination of the final baryon asymmetry requires a precise understanding of the function f , i.e., of the temperature dependence of the weak mixing angle. The latest lattice studies of the electroweak crossover, however, have a relatively large uncertainty, as far as the exact evolution of $\theta_W(T)$ is concerned [85]. Moreover, there is a relatively large discrepancy between the numerical results and the one-loop perturbative analytical estimate [86]. For this reason, we shall follow [64] and simply model θ_W in terms of a smooth step function,

$$\cos^2 \theta_W = \cos^2 \theta_W^0 + \frac{1 - \cos^2 \theta_W^0}{2} \left[1 + \tanh \left(\frac{T - T_{\text{step}}}{\Delta T} \right) \right], \quad \cos^2 \theta_W^0 = \frac{g_W^2}{g_W^2 + g_Y^2} \simeq 0.77, \quad (60)$$

¹³Here we consider the case where the hypermagnetic field enters the inverse cascade regime prior to EWSB.

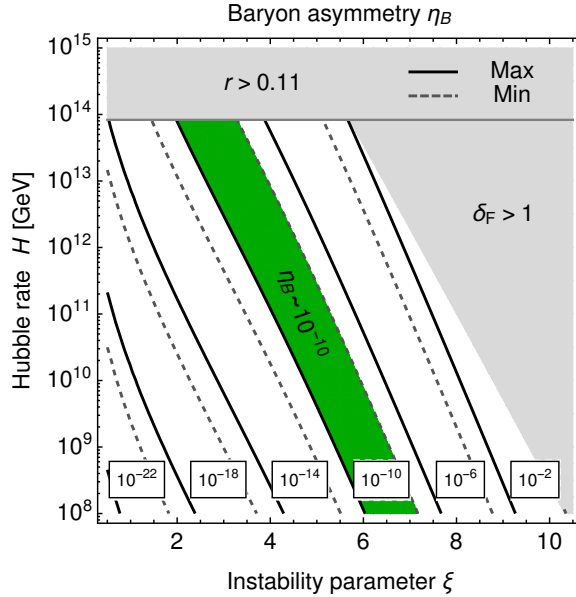


Figure 5: Baryon asymmetry $\eta_B = n_B/s$ as a function of the instability parameter ξ and the Hubble rate H ; see Eq. (62). Here, both ξ and H are understood to correspond to the respective values at the end of inflation, $\xi \equiv \xi_{\text{rh}}$ and $H \equiv H_{\text{rh}}$. The black solid [gray dashed] contours correspond to the maximally [minimally] allowed value of the function f ; see Eq. (61). The green band illustrates the region in parameter space where η_B is in accord with the observed value, $\eta_B^{\text{obs}} \sim 10^{-10}$. The gray-shaded regions are the same as in Fig. 2.

which we believe to cover all realistic values of the function f including its uncertainties. Our phenomenological ansatz reflects the fact that, at $T \sim T_{\text{step}}$, the weak mixing angle changes from its high-temperature value in the symmetric phase, $\cos^2 \theta_W = 1$, to its low-temperature value in the Higgs phase, $\cos^2 \theta_W = \cos^2 \theta_W^0$. The width of this transition in temperature space is characterized by the parameter ΔT . Realistic values of T_{step} and ΔT fall into the ranges $155 \text{ GeV} \lesssim T_{\text{step}} \lesssim 160 \text{ GeV}$ and $5 \text{ GeV} \lesssim \Delta T \lesssim 20 \text{ GeV}$, respectively. Varying T_{step} and ΔT within these ranges, we find that the realistic values of f almost span three orders of magnitude,

$$5.6 \times 10^{-4} \lesssim f(\theta_W, T_{\text{BAU}}) \lesssim 0.32, \quad (61)$$

which translates into an uncertainty in the final baryon asymmetry,

$$\eta_B \simeq (1.9 \times 10^{-3} \dots 1.1) \times 10^{-16} \left(\frac{e^{2\pi\xi_{\text{rh}}}}{\xi_{\text{rh}}^4} \right) \left(\frac{H_{\text{rh}}}{10^{13} \text{ GeV}} \right)^{3/2}. \quad (62)$$

This expression for η_B is one of the main results of our paper. We show η_B as a function of H_{rh} and ξ_{rh} in Fig. 5. Evidently, the observed baryon asymmetry, $\eta_B^{\text{obs}} \sim 10^{-10}$ [87], can be reproduced in a large part of parameter space. In view of Fig. 5, several comments are in order:

(i) For most values of the Hubble rate at the end of inflation, H_{rh} , the instability parameter ξ_{rh} needs to take a value in the range $4 \lesssim \xi_{\text{rh}} \lesssim 6$ to allow for successful baryogenesis. According to Eq. (32), this requires the suppression scale Λ to take a value in the following interval,

$$2.9 \times 10^{17} \text{ GeV} \lesssim \Lambda \lesssim 4.3 \times 10^{17} \text{ GeV}. \quad (63)$$

In other words, the requirement of successful baryogenesis roughly fixes the value of the suppression scale Λ in the axion-gauge-field coupling, $\Lambda \sim 3 \times 10^{17}$ GeV. This is within a factor of 10 of the Planck scale, which indicates that the axion needs to be coupled rather weakly.

(ii) With $\Lambda \sim 3 \times 10^{17}$ GeV and given the location of the green band in Fig. 5, it is clear that successful baryogenesis is incompatible with large values of δ_F and δ_{KG} ; see Fig. 2 and Eq. (23). This means that, in the case of successful baryogenesis, the gauge field production during inflation is never going to dominate the inflationary dynamics. Conversely, this can be rephrased by saying that inflationary scenarios that eventually do lead to $\delta_F \sim 1$ unavoidably result in an overproduction of baryon number.¹⁴ Of course, this problem can be trivially solved by re-interpreting the axion coupling to the hypercharge gauge fields as a coupling to the gauge fields of some other, hidden $U(1)$. But this solution comes at a high cost: If we replaced $U(1)_Y$ by some hidden $U(1)'$, we would have to give up on primordial magnetogenesis and baryogenesis via decaying hypermagnetic helicity as well. That is, we might still be able to generate a sizable signal in GWs (see Sec. 4.2); but we would lose all other virtues of our scenario.

(iii) The parameter region consistent with successful baryogenesis is also marked in Fig. 4. As can be seen from this figure, successful baryogenesis around the time of EWSB correlates with a particular strength of the large-scale magnetic fields in the present epoch, $B_p^0 \sim 10^{-16}$ GeV. Note that this is the value that we already anticipated in Eq. (4).

(iv) Our result in Fig. 5 presents an update of earlier studies in the literature [61, 65]. In comparison to these earlier works, we find that successful baryogenesis apparently requires larger values of H_{rh} as well as larger values of ξ_{rh} . Otherwise, the produced asymmetry will fall short of the observed value by several orders of magnitude. The reason for this change in numbers is that we indirectly include several effects in our analysis that had previously been neglected. By employing the analytical expression in Eq. (58), we make sure to account for the gradual change of the weak mixing angle during the electroweak crossover, the chiral magnetic effect, the standard model Yukawa interactions, etc. The combination of Eq. (58) with our results for B_p and λ_p at the time of EWSB (see Eqs. (47) and (48)) then enables us to assess the efficiency of baryogenesis more accurately. On the other hand, it must not be forgotten that also our analysis still suffers from quite large uncertainties. Future work needs to tackle in particular two issues: a better treatment of reheating after inflation as well as a better understanding of the evolution of the weak mixing angle during the electroweak phase transition. Moreover, to relate the efficiency of baryogenesis to the strength of the present-day intergalactic magnetic fields more precisely, more work on the evolution of magnetic fields at low temperature is needed.

¹⁴This conclusion can be avoided if the reheating temperature after inflation is below the electroweak scale, $T_{\text{rh}} \lesssim 100$ GeV. In this case, baryon number is not anomalously violated after inflation and the decaying *magnetic* (not hypermagnetic) helicity fails to generate a nonzero baryon asymmetry. Similarly, our conclusions regarding the overproduction of baryon number may change if the dynamics of reheating, which we did not account for in our analysis, should dramatically change our estimate of the initial hypermagnetic field strength in Eq. (35).

4.2 High-frequency signal in gravitational waves

In Sec. 2.1, we discussed the equations of motion for the homogeneous background fields a and A_{\pm}^k in an exact FLRW background; see Eqs. (6), (9) and (13). In addition to this, it is also essential to study the dynamics of the corresponding perturbations in the inflaton field as well as in the metric tensor. Here, a crucial observation is that the exponentially enhanced gauge field readily provides new source terms for the primordial scalar and tensor perturbations [23, 24]. As it turns out, the new contributions to the scalar power spectrum are mostly controlled by the backreaction parameter δ_{KG} ; see, e.g., [44]. As long as we stay in the weak field regime, $\delta_{\text{KG}} \ll 1$ (see Eq. (23)), the corrections to the scalar power spectrum are, therefore, more or less negligible for our purposes. The corrections to the tensor power spectrum, on the other hand, can become quite sizable from the point of view of observational prospects—and that even so in the weak field regime! In fact, primordial tensor perturbations from the epoch of inflation give rise to a spectrum of stochastic GWs in the present epoch over a broad range of frequencies. The amplification of the tensor power spectrum in models of pseudoscalar inflation, therefore, has important consequences for the expected signal of stochastic GWs from inflation. As shown in [21, 22], pseudoscalar inflation may even result in sizable GWs on small scales that are possibly within the reach of direct GW observations. As we will discuss in the following, the primordial GW signal on small scales ends up being dominated by the gauge contribution rather than the vacuum contribution in a large part of parameter space. This opens up the possibility to test our scenario, at least in principle, by means of future GW observations.

Let us now discuss the spectral GW energy density from inflation, $\Omega_{\text{GW}}^0 h^2$, in more detail. We first argue that the GW spectrum is flat to first approximation. In the presence of the axion-gauge-field coupling in Eq. (2), the spectral energy density $\Omega_{\text{GW}}^0 h^2$ receives two contributions,

$$\Omega_{\text{GW}}^0 h^2 = [\Omega_{\text{GW}}^0 h^2]_{\text{vacuum}} + [\Omega_{\text{GW}}^0 h^2]_{\text{gauge}} . \quad (64)$$

Here, $[\Omega_{\text{GW}}^0 h^2]_{\text{vacuum}}$ denotes the vacuum contribution in standard single-field slow-roll inflation,

$$[\Omega_{\text{GW}}^0 h^2]_{\text{vacuum}} = \frac{\Omega_{\text{rad}}^0 h^2}{12} \left(\frac{g_*}{g_*^0} \right) \left(\frac{g_{*,s}^0}{g_{*,s}} \right)^{4/3} \left(\frac{H}{\pi M_{\text{Pl}}} \right)^2 , \quad (65)$$

which scales with the square of Hubble rate during inflation. $\Omega_{\text{rad}}^0 h^2 \simeq 2.5 \times 10^{-5}$ is the density parameter of radiation in the present epoch, while the combination of effective numbers of DOFs ($g_* = 106.75$, $g_*^0 = 2$, $g_{*,s} = 106.75$, $g_{*,s}^0 \simeq 3.91$) accounts for the redshift behavior of the GW signal since its production.¹⁵ For typical values of H , Eq. (65) yields a rather weak GW signal,

$$[\Omega_{\text{GW}}^0 h^2]_{\text{vacuum}} \simeq 2.3 \times 10^{-22} \left(\frac{H}{10^{11} \text{ GeV}} \right)^2 . \quad (66)$$

¹⁵More precisely, these factors are part of the so-called transfer function, which describes the redshift behavior of GW modes outside and inside the Hubble horizon; see, e.g., [88] and references therein. Strictly speaking, the functional form of Eq. (65) only applies to those modes which cross inside the Hubble horizon prior to matter-radiation equality. This is however the case for all GW modes that we are going to be interested in.

Recalling that the Hubble rate during inflation is related to the primordial tensor-to-scalar ratio, $H \simeq 7.9 \times 10^{13} \text{ GeV} (r/0.1)^{1/2}$, we point out that Eq. (66) is in fact equivalent to Eq. (1).

Meanwhile, one obtains for the contribution to $\Omega_{\text{GW}}^0 h^2$ [23, 24] from the gauge fields,

$$[\Omega_{\text{GW}}^0 h^2]_{\text{gauge}} \simeq [\Omega_{\text{GW}}^0 h^2]_{\text{vacuum}} \left(\frac{H}{M_{\text{Pl}}} \right)^2 (f_L + f_R) e^{4\pi\xi}, \quad (67)$$

where f_L and f_R are two fit functions that need to be determined numerically,¹⁶

$$f_L = 10^{-7} \times \begin{cases} 2.6 / \xi^{5.7} & ; \quad \xi \lesssim 3 \\ 4.3 / \xi^{6.0} & ; \quad \xi \gtrsim 3 \end{cases}, \quad f_R = \frac{9.2}{\xi^{6.0}} \times 10^{-10}. \quad (68)$$

Fitting Eq. (67) as a function of H^4 and $e^{4\pi\xi}$ results in the following phenomenological expression, which reproduces the exact result very accurately in the entire parameter space of interest,

$$[\Omega_{\text{GW}}^0 h^2]_{\text{gauge}} \simeq 2.3 \times 10^{-22} \exp[0.91 \times 4\pi(\xi - 4.61)] \left(\frac{H}{10^{11} \text{ GeV}} \right)^4. \quad (69)$$

Note that, in Eqs. (66) and (69), we have chosen the reference values for H and ξ such that both contributions to the GW spectrum are of the same size. Moreover, Eqs. (66) and (69) also illustrate that, for $H = 10^{11} \text{ GeV}$ and $\xi > 4.61$, the gauge contribution to $\Omega_{\text{GW}}^0 h^2$ exceeds the vacuum contribution. This demonstrates that the GW signal can indeed be dominated by the gauge contribution, although both backreaction parameters, δ_{F} and δ_{KG} , actually take small values; see Eq. (22). In fact, it is easy to show that the GW spectrum is always dominated by the gauge contribution as soon as H is larger than some critical, ξ -dependent value $H_{\text{GW}}^{\text{crit}}$,

$$H_{\text{GW}}^{\text{crit}} = (f_L + f_R)^{-1/2} e^{-2\pi\xi} M_{\text{Pl}} \simeq 1.1 \times 10^{10} \text{ GeV} \exp[-0.88 \times 2\pi(\xi - 5)]. \quad (70)$$

As long as ξ and H are constant, both $[\Omega_{\text{GW}}^0 h^2]_{\text{vacuum}}$ and $[\Omega_{\text{GW}}^0 h^2]_{\text{gauge}}$ are independent of time t and frequency f . In this limit, GWs therefore exhibit a flat power spectrum.

Next, let us discuss the frequency dependence of this spectrum. We just saw that the GW spectrum is flat in the limit where ξ and H are constant. However, ξ and H are not *exactly* constant but slowly vary during inflation. This results in a frequency dependence of the GW spectrum, after all. A GW signal at frequency f corresponds to a primordial tensor perturbation with wavenumber $k = 2\pi R_0 f$, where R_0 denotes the present-day value of the scale factor. During inflation, the amplitude of this perturbation mode freezes out once it is sufficiently far outside the Hubble horizon, if there are no active sources on *super*-horizon scales. In standard slow-roll inflation without any additional coupling to gauge fields, this requirement is satisfied simply once the k mode exits the horizon at $k/R(t_k) = H(t_k)$ (where t_k is defined by this very relation). In this case, one finds the GW amplitude at frequency f by evaluating the spectral energy density $\Omega_{\text{GW}} h^2$ for $R(t_k) H(t_k) = k = 2\pi R_0 f$. On the other hand, it is not *a priori* clear whether this statement also remains true if the inflaton couples to gauge fields. The axion-gauge-field coupling

¹⁶In Sec. 2.2, we solved all relevant momentum integrals by ourselves; see Eq. (20). However, in our discussion of the primordial tensor perturbations, we will now rely on the numerical fit functions available in the literature.

may, e.g., affect the evolution of the tensor modes even on *super*-horizon scales. However, for $\xi \sim \mathcal{O}(1)$, it turns out that the k mode of the gauge field as well as the tensor perturbations of the metric are amplified only around the time of horizon exit. We therefore conclude that the GW spectrum at wavenumber k is generated and fixed once the k mode exits the horizon. For this reason, we can simply evaluate ξ and H in Eq. (67) at the time of horizon exit,

$$\xi = \xi(t_k), \quad H = H(t_k), \quad R(t_k)H(t_k) = k = 2\pi R_0 f. \quad (71)$$

Since both ξ and H slightly vary with time during inflation, this procedure results in a *frequency-dependent* spectrum of stochastic GWs. The contribution from the gauge fields has an exponential dependence on ξ , which results in a peak in the GW spectrum when ξ is maximal.

The present frequency f of the GW mode with wavenumber $k = 2\pi R_0 f$ is related to the number of e -folds between the time of horizon exit and the end of inflation, N_e , as follows,

$$N_e(f) = \ln \left[\frac{1}{2\pi f} \left(\frac{\pi^2 g_* g_{*,s}^0}{45 g_{*,s}} \right)^{1/3} \frac{T_0 T_{\text{rh}}^{1/3} H_{\text{inf}}^{1/3}}{M_{\text{Pl}}^{2/3}} \right], \quad (72)$$

where $H_{\text{inf}} \approx H_{\text{rh}}$ is the Hubble rate during inflation. In the approximation of instant reheating, $T_{\text{rh}} = \sqrt{M_* H_{\text{rh}}}$, this expression reduces to

$$N_e(f) \simeq 2.0 + \frac{1}{2} \ln \left(\frac{H_{\text{rh}}}{10^{11} \text{ GeV}} \right) - \ln \left(\frac{f}{1 \text{ MHz}} \right). \quad (73)$$

Then, we obtain the frequency-dependent GW spectrum as the following expression,

$$\Omega_{\text{GW}} h^2(f) = \Omega_{\text{GW}} h^2(\xi(N_e(f)), H(N_e(f))). \quad (74)$$

The interplay between both contributions to the GW spectrum is depicted in Fig. 6, where we plot the total spectral energy density $\Omega_{\text{GW}}^0 h^2$ as a function of ξ and H that slightly vary during inflation.¹⁷ Each inflation model defines a trajectory γ in the ξ - H plane that may, e.g., be parametrized in terms of the number of e -folds until the end of inflation,

$$\gamma = \{(\xi(N_e), H(N_e)) \forall N_e\}. \quad (75)$$

γ passes through various values of $\Omega_{\text{GW}}^0 h^2$ during inflation. For each model, this results in a characteristic spectrum of stochastic GWs that could, in principle, be still observed today.

For many models of pseudoscalar inflation, ξ grows towards the end of inflation, as the inflaton velocity \dot{a} becomes larger and larger. If this growth in ξ is strong enough, such that $H > H_{\text{GW}}^{\text{crit}}$ at some point (see Eq. (70)), the gauge contributions to $\Omega_{\text{GW}} h^2$ will result in an exponentially steep increase in the GW spectrum. This mechanism of GW production will shut off as soon as inflation is over and our mechanism of gauge field production is no longer active. All in all, we therefore expect a characteristic feature in the GW spectrum associated with the

¹⁷During slow-roll inflation, ξ and H vary only very slowly, such that their time dependence does not have a strong impact on the gauge field evolution. This is the reason why we are able to solve Eq. (15) for constant ξ .

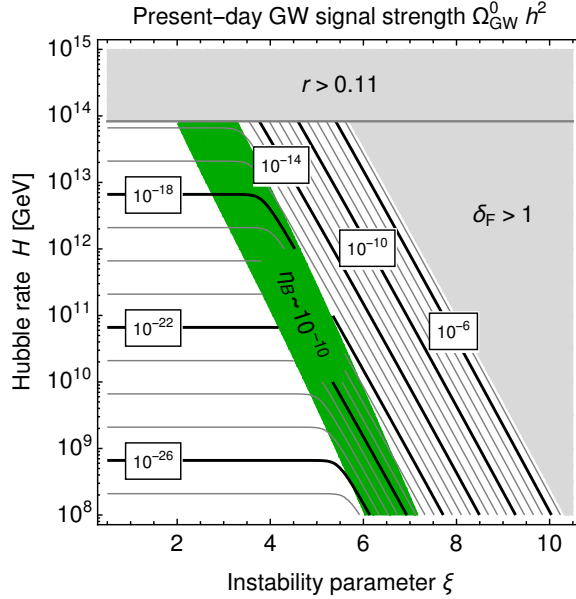


Figure 6: Present-day GW signal strength $\Omega_{\text{GW}}^0 h^2$ as a function of the instability parameter ξ and the Hubble rate H ; see Eqs. (64), (65), and (67). Here, ξ and H correspond to free parameters, which vary in the course of inflation. The green band is the same as in Figs. 4 and 5. The gray-shaded regions are the same as in Fig. 2.

explosive gauge field production at the end of inflation, i.e., around $N_e \simeq 0$. According to Eq. (73), we estimate that this peak should occur at frequencies in the MHz range or at even higher frequencies,

$$N_e(f_{\text{peak}}) \simeq 0 \quad \Rightarrow \quad f_{\text{peak}} \simeq 7.1 \text{ MHz} \left(\frac{H_{\text{rh}}}{10^{11} \text{ GeV}} \right)^{1/2}. \quad (76)$$

To estimate the strength of the peak in the GW spectrum, we simply need to evaluate $\Omega_{\text{GW}} h^2$ in Eq. (64) for $\xi = \xi_{\text{rh}}$ and $H = H_{\text{rh}}$. Or alternatively, we may trade the dependence on ξ_{rh} and H_{rh} for the present-day strength of the magnetic field, B_p^0 , as well as the peak frequency, f_{peak} . Making use of Eqs. (50), (64), and (76), we then find the following numerical relation,

$$[\Omega_{\text{GW}}^0 h^2]_{\text{peak}} \simeq 3.2 \times 10^{-20} \left(\frac{B_p^0}{10^{-16} \text{ GeV}} \right)^{6.13} \left(\frac{f_{\text{peak}}}{10 \text{ MHz}} \right)^{1.87}, \quad (77)$$

which is another main result of our paper. In order to eliminate the ξ dependence in $\Omega_{\text{GW}} h^2$, we numerically solved Eq. (50) for ξ . Based on the relation in Eq. (77), we plot B_p^0 as a function of f_{peak} and $[\Omega_{\text{GW}}^0 h^2]_{\text{peak}}$ in Fig. 7. In view of Eq. (77) and Fig. 7, several comments are in order:

(i) In scenarios consistent with successful baryogenesis, the gauge field production at the end of inflation is typically accompanied by a rather weak signal in GWs at high frequencies. The detection of this peak is certainly out of reach of present-day technology. On the other hand, it is an unavoidable consequence of primordial magnetogenesis in our scenario. In the future, the detection of such a GW peak may therefore serve as a smoking-gun signal of primordial magnetogenesis at the end of pseudoscalar inflation. This in turn would lend support to the idea of baryogenesis from decaying hypermagnetic helicity. In particular, one could assess whether

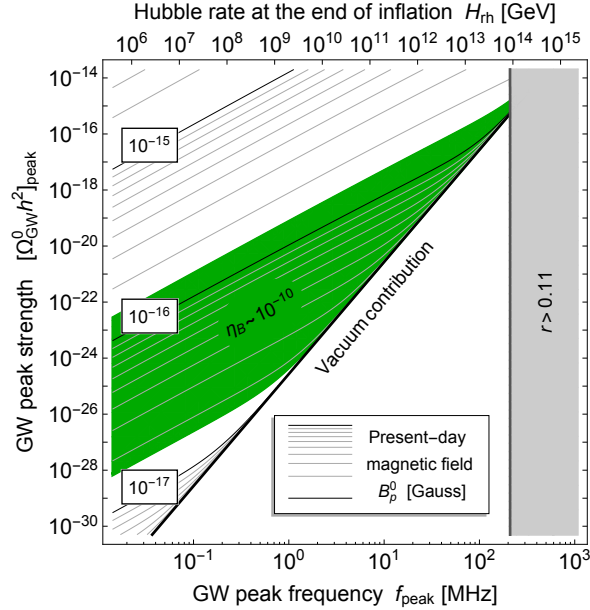


Figure 7: Present-day magnetic field strength B_p^0 as a function of the peak frequency f_{peak} and the strength of the peak in the GW spectrum associated with the gauge field production at the end of inflation, $[\Omega_{\text{GW}}^0 h^2]_{\text{peak}}$; see Eq. (77). In the approximation of instant reheating, f_{peak} is directly related to the Hubble rate at the end of inflation; see Eq. (76). The green band illustrates the region in parameter space where $\eta_B \sim 10^{-10}$; see Eq. (62).

the strength of the observed GW signal turns out to be consistent with an inflaton coupling to the hypercharge gauge field — or whether this assumption would lead to baryon overproduction.

(ii) Along the diagonal line in Fig. 7, the GW spectrum at the end of inflation is dominated by the (irreducible) vacuum contribution. The part of parameter space below this line is therefore not accessible. Meanwhile, the vertical distance between this line and any point above indicates the extent to which the peak in the GW spectrum sticks out of the usual vacuum background.

(iii) We stress once more that, at the quantitative level, Eq. (77) and Fig. 7 may still receive a number of corrections. After all, every quantity in our analysis (B_p^0 , λ_p^0 , η_B , and $\Omega_{\text{GW}}^0 h^2$) comes with potentially large uncertainties. Nonetheless, we believe that Eq. (77) and Fig. 7 convey the correct idea at the qualitative level. Our results illustrate that pseudoscalar inflation leads to a highly nontrivial relation between initially completely independent phenomena: the present-day strength of the intergalactic magnetic field, the baryon asymmetry of the universe, and the stochastic background of GWs. This realization is one of our main achievements in this paper.

5 Explicit scenarios based on natural inflation

All quantities that we were interested in so far (B_p^0 , λ_p^0 , η_B , and $\Omega_{\text{GW}}^0 h^2$) solely depend on the values of ξ and H at the end of inflation. This observation allowed us to perform a completely model-independent analysis up to this point. We did not specify the form of the inflaton potential $V(a)$ and discarded all details of the reheating process. Instead, we simply employed a model-

independent parametrization in terms of ξ_{rh} and H_{rh} . This means that all of our results up to this point apply to any model of pseudoscalar inflation that is anomalously coupled to the standard model hypercharge sector. Now, however, we shall illustrate our results by means of concrete examples, in order to see how realistic models of inflation give rise to the phenomenology described in the previous sections. To this end, we shall now study the evolution of ξ and H during inflation in concrete models and illustrate how they approach certain values towards the end of inflation. In other words: up to now, we were only interested in certain points in the ξ - H parameter plane; now we turn to the *inflationary trajectories* in this parameter plane.

Given the Lagrangian in Eq. (5), the inflaton field a is naturally identified as an axion, *i.e.*, the PNCB of a spontaneously broken global symmetry G_{global} . If this symmetry is anomalous under the standard model hypercharge gauge group $U(1)_Y$, the axion a will couple to the standard model hypercharge gauge field just as in Eq. (2). Moreover, if G_{global} is *in addition* anomalous under some strongly coupled gauge symmetry G_{strong} , nonperturbative effects in the G_{strong} gauge sector will generate a scalar potential for a of the following form,

$$V(a) = m_a^2 f_a^2 \left[1 - \cos\left(\frac{a}{f_a}\right) \right]. \quad (78)$$

Here, m_a and f_a denote the axion mass as well as the axion decay constant. The overall scale of the axion potential is set by the confinement scale in the strongly coupled sector, $m_a^2 f_a^2 \sim \Lambda_{\text{strong}}^4$. In the following, we can treat both m_a and f_a as free parameters. The scalar potential in Eq. (78) is nothing but the scalar potential of natural inflation [25, 26]. This is a trivial statement given the fact that natural inflation denotes the very idea that inflation is driven by the PNCB of some spontaneously broken and anomalous global symmetry. In the following, we shall study the inflationary trajectory for natural inflation in the ξ - H plane.

For any value of the inflaton field during slow-roll inflation, one can determine (ξ, H) from Eqs. (6) and (9). Once we replace \dot{a} by $2\Lambda H\xi$, see Eq. (14), and neglect \ddot{a} , we have

$$\begin{aligned} 3M_{\text{Pl}}^2 H^2 - \frac{1}{2} (2\Lambda H\xi)^2 - V - \frac{1}{2} [\rho_{EE}(\xi, H) + \rho_{BB}(\xi, H)] &= 0, \\ 6\Lambda H^2 \xi + \frac{dV}{da} - \frac{1}{\Lambda} \rho_{EB}(\xi, H) &= 0. \end{aligned} \quad (79)$$

For a given pair of values for $(V, \frac{dV}{da})$ as well as for given Λ , we can numerically solve Eq. (79) for (ξ, H) . The slow-roll parameter ε including the contribution of the gauge field is [39]

$$\varepsilon = -\frac{\dot{H}}{H^2} = \frac{1}{2M_{\text{Pl}}^2 H^2} \left[\dot{a}^2 + \frac{2}{3} (\rho_{EE} + \rho_{BB}) \right], \quad (80)$$

which can be computed once (ξ, H) has been determined. For each field value, we are therefore able to compute the corresponding value of ε . With the aid of Eq. (80), we can hence numerically determine the end point of inflation, where $\varepsilon = 1$. The number of e-folds N_e is given by

$$N_e = \int_{a_{\text{end}}}^a da \frac{dN_e}{da}, \quad (81)$$

where a_{end} is the field value at the end of inflation and the integrand is a simple function of ξ ,

$$\frac{dN_e}{da} = -\frac{H}{\dot{a}} = -\frac{1}{2\Lambda\xi}. \quad (82)$$

In summary, for each inflaton field value, we can compute the quadruplet $(\xi, H, \varepsilon, N_e)$, which enables us to draw an inflationary trajectory for any given model in the ξ - H parameter plane.

Now let us compute some explicit examples. Our variant of the natural inflation model is characterized by three parameters: the two parameters (m_a, f_a) in the potential, see Eq. (78), as well as the suppression scale Λ in the Chern-Simons interaction. We take the following values:¹⁸

$$\text{Model A:} \quad m_a^2 = 4.1 \times 10^{-11} M_{\text{Pl}}^2, \quad f_a = 7.0 M_{\text{Pl}}, \quad \Lambda^{-1} = 5.6 M_{\text{Pl}}^{-1}. \quad (83)$$

Here, to distinguish it from other models that will be discussed, we refer to it as model A. Note that, to ensure successful baryogenesis, Λ cannot be chosen arbitrarily; see Eq. (63). Besides, to make the model compatible with the CMB observations, we need to chose particular values for the two parameters m_a and f_a . The parameters in Eq. (83) have been tuned in such a way that the model is compatible with all CMB observations and the baryon number asymmetry.

Following the procedure introduced above, we numerically compute (ξ, H) by solving Eq. (79) for each field value in the relevant part of the potential with a step width of $\Delta a = 0.01 M_{\text{Pl}}$. Then we compute the slow-roll parameter ε to determine the end of inflation, which is at

$$\text{Model A:} \quad a_{\text{end}} = -0.94 M_{\text{Pl}}. \quad (84)$$

For all field values during inflation, $a < a_{\text{end}}$, the number of e-folds N_e is computed according to Eq. (81). Together, these points form the trajectory corresponding to model A in Fig. 8.

The scalar power spectrum is evaluated according to

$$P_s = \left(\frac{H^2}{2\pi\dot{a}} \right)^2 \left(\frac{k}{k_{\text{CMB}}} \right)^{n_s-1}, \quad (85)$$

where $k_{\text{CMB}} = 0.05 \text{ Mpc}^{-1}$ is the CMB pivot scale; and H and \dot{a} are evaluated at the time when the pivot scale exits the horizon. We neglect the contribution from the gauge fields, since it is negligibly small in the region of interest. This should be compatible with the CMB normalization [15]:

$$P_s^{\text{obs}} = (2.21 \pm 0.07) \times 10^{-9}. \quad (86)$$

The CMB pivot scale exits the horizon at $N_e^{\text{CMB}} \simeq 55$, where we obtain

$$\text{Model A:} \quad a = -13.4 M_{\text{Pl}}, \quad \dot{a} = 3.0 \times 10^{-6} M_{\text{Pl}}^2, \quad H = 3.0 \times 10^{-5} M_{\text{Pl}}, \quad \xi = 0.28. \quad (87)$$

With these numerical results, we can evaluate the scalar power spectrum:

$$\text{Model A:} \quad P_s = 2.3 \times 10^{-9}, \quad (88)$$

¹⁸The parameters f_a and Λ ought to be related to each other in the UV completion of our model. But in this study, we do not specify any UV physics, which is why we treat f_a and Λ as independent parameters.

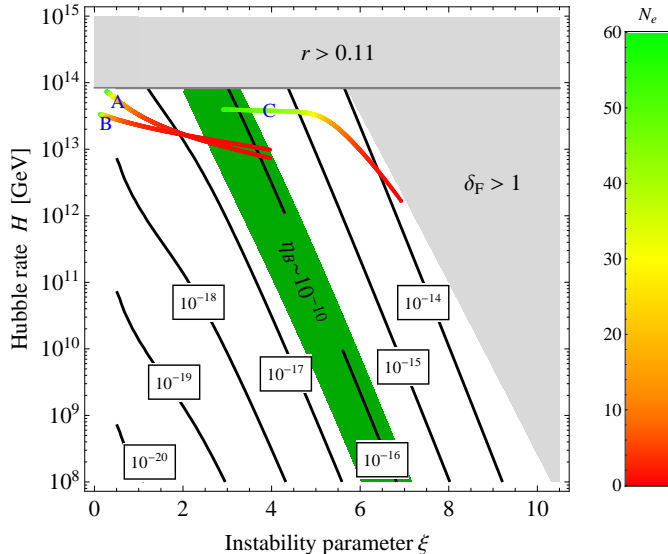


Figure 8: Trajectories of several inflation models in the ξ - H parameter plane. Trajectory A corresponds to natural inflation, see Eqs. (78) and (83), while trajectories B and C correspond to Starobinsky inflation, see Eq. (90), in the case of small and large axion-gauge-fields coupling, respectively. Numerical details are listed in Tab. 1. Successful baryogenesis is accomplished for any inflationary trajectory that ends in the green band, i.e., if the point $(\xi, H)_{\text{end}} = (\xi_{\text{rh}}, H_{\text{rh}}) = (\xi(N_e = 0), H(N_e = 0))$ lies in the green band; see Fig. 4 and Eq. (62).

which is compatible with Eq. (86). Since the gauge field contribution is very weak at $N_e = N_e^{\text{CMB}}$, the spectral index n_s and the tensor-to-scalar ratio r can be evaluated in the conventional way:

$$\text{Model A:} \quad n_s = 1 + 2\eta - 6\varepsilon \simeq 0.96, \quad r = 16\varepsilon \simeq 0.08. \quad (89)$$

which agrees with the current PLANCK constraints [15]. All of the above numerical results are summarized in Tab. 1.

We can further compute the GW spectrum according to Eq. (64), including both the vacuum and gauge contributions. This is shown by the red curve in Fig. 9, where the red shadow denotes the gauge contribution. In Fig. 9, we also present the current constraints from advanced LIGO and future sensitivities from advanced LIGO and LISA. It turns out that the GW energy density $\Omega_{\text{GW}}^0 h^2$ produced in model A is far below the reach of current or upcoming GW interferometers.

It has been shown [21] however that, with a strongly coupled axion, some models could reach the sensitivity of current or upcoming GW interferometers. For the Starobinsky model [5], e.g.,

$$V_{\text{Starobinsky}}(a) = V_0 (1 - e^{\gamma_s a})^2, \quad a < 0, \quad (90)$$

with $(V_0, \gamma_s) = (1.0 \times 10^{-9} M_{\text{Pl}}^4, 0.3 M_{\text{Pl}}^{-1})$ and an axion-gauge-field coupling $\Lambda^{-1} = 75 M_{\text{Pl}}^{-1}$ (which is more than 10 times larger than the case we just discussed), $\Omega_{\text{GW}}^0 h^2$ can reach the future sensitivities of advanced LIGO and LISA, as shown by the black curve in Fig. 9. Such a large GW energy is due to a very strong axion-gauge-field coupling, which transfers almost the entire energy carried by the inflaton into the gauge field and induces much larger tensor perturbations.

Model	A	B	C
Λ^{-1}	$5.6 M_{\text{Pl}}^{-1}$	$5.6 M_{\text{Pl}}^{-1}$	$75 M_{\text{Pl}}^{-1}$
$V(a)$	Eq. (78)	Eq. (90)	Eq. (90)
$\begin{bmatrix} m_a^2 \\ f_a \end{bmatrix}$ or $\begin{bmatrix} V_0 \\ \gamma_s \end{bmatrix}$	$\begin{bmatrix} 4.1 \times 10^{-11} M_{\text{Pl}}^2 \\ 7.0 M_{\text{Pl}} \end{bmatrix}$	$\begin{bmatrix} 6.7 \times 10^{-10} M_{\text{Pl}}^4 \\ 0.30 M_{\text{Pl}}^{-1} \end{bmatrix}$	$\begin{bmatrix} 1.0 \times 10^{-9} M_{\text{Pl}}^4 \\ 0.30 M_{\text{Pl}}^{-1} \end{bmatrix}$
$\begin{bmatrix} a \\ \dot{a} \\ H \\ \xi \end{bmatrix}_{N_e=0}$	$\begin{bmatrix} -0.94 M_{\text{Pl}} \\ 4.3 \times 10^{-6} M_{\text{Pl}}^2 \\ 3.0 \times 10^{-6} M_{\text{Pl}} \\ 4.0 \end{bmatrix}$	$\begin{bmatrix} -0.83 M_{\text{Pl}} \\ 5.7 \times 10^{-6} M_{\text{Pl}}^2 \\ 4.0 \times 10^{-6} M_{\text{Pl}} \\ 4.0 \end{bmatrix}$	$\begin{bmatrix} -0.09 M_{\text{Pl}} \\ 1.3 \times 10^{-7} M_{\text{Pl}}^2 \\ 6.9 \times 10^{-7} M_{\text{Pl}} \\ 6.9 \end{bmatrix}$
$\begin{bmatrix} a \\ \dot{a} \\ H \\ \xi \end{bmatrix}_{N_e=55}$	$\begin{bmatrix} -13 M_{\text{Pl}} \\ 3.0 \times 10^{-6} M_{\text{Pl}}^2 \\ 3.0 \times 10^{-5} M_{\text{Pl}} \\ 0.28 \end{bmatrix}$	$\begin{bmatrix} -8.7 M_{\text{Pl}} \\ 6.7 \times 10^{-7} M_{\text{Pl}}^2 \\ 1.4 \times 10^{-5} M_{\text{Pl}} \\ 0.13 \end{bmatrix}$	$\begin{bmatrix} -7.2 M_{\text{Pl}} \\ 1.3 \times 10^{-6} M_{\text{Pl}}^2 \\ 1.6 \times 10^{-5} M_{\text{Pl}} \\ 2.9 \end{bmatrix}$
$\begin{bmatrix} P_s \\ n_s \\ r \end{bmatrix}_{N_e=55}$	$\begin{bmatrix} 2.3 \times 10^{-9} \\ 0.96 \\ 0.08 \end{bmatrix}$	$\begin{bmatrix} 2.1 \times 10^{-9} \\ 0.97 \\ 0.02 \end{bmatrix}$	$\begin{bmatrix} 2.2 \times 10^{-9} \\ 0.94 \\ 0.05 \end{bmatrix}$

Table 1: Various parameters and numerical results for the three models A, B, and C.

But strong axion-gauge-field couplings will always lead to baryon overproduction, as discussed model-independently in Sec. 4; see Eq. (63). Indeed, Fig. 8 shows that the trajectory of this model (we refer to it as model C; for numerical details, see Tab. 1) ends at a point far away from the region for successful baryogenesis (the green band). Actually, this point is very close to the bound $\delta_{\text{F}} = 1$, which corresponds to the situation that the entire energy of the universe is stored in the gauge field. If we reduce the axion-gauge-field coupling of model C to the same value as in model A, then the model (now referred to as model B) leads to successful baryogenesis; see Fig. 8. But it has small $\Omega_{\text{GW}}^0 h^2$, approximately of the same order of magnitude as model A.

It is interesting to note that the GW spectra of model A and B both peak at the very end of inflation, where the gauge contributions become dominant (at $0 \lesssim N_e \lesssim 0.3$, corresponding to $f \sim 40$ MHz, see the right panel of Fig. 9). This is an important feature of these models compared to models without the inflaton-gauge-field coupling. Although these peaks are out of reach of conventional GW interferometers, once detected by some other new technology in the future, they may serve as a smoking-gun signal for baryogenesis via primordial magnetic fields.

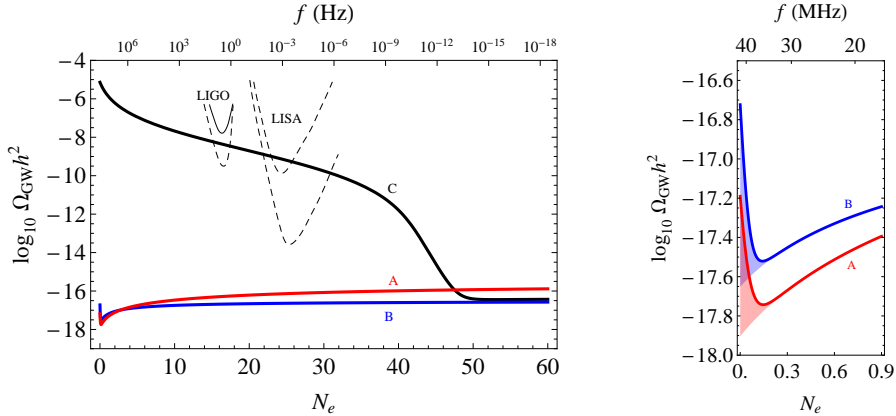


Figure 9: GW spectra of several models compared to the current (solid lines) and future (dashed lines) constraints from advanced LIGO and LISA. The red, blue and black curves corresponds to models A, B, and C, respectively. Model A: natural inflation; model B/C: Starobinsky inflation with a small/large axion-gauge-field coupling; see Tab. 1 for the numerical details. The red and blue shadows in the right panel represent the gauge contributions. To relate the number of e-folds N_e and the frequency f we have used Eq. (73) with $H_{\text{rh}} = 10^{12.5}$ GeV, which is approximately correct for the models A, B, and C.

6 Conclusions

In this paper, we revisited the implications of a Chern-Simons-like inflaton coupling to the standard model hypercharge gauge field, $\mathcal{L} \supset a/(4\Lambda) F\tilde{F}$, in general models of pseudoscalar inflation. We focused in particular on two phenomenological aspects: (i) the production of primordial gauge fields towards the end of inflation (i.e., primordial magnetogenesis) and its consequences for baryogenesis from decaying (hyper)magnetic fields at the time of EWSB; and (ii) the associated production of primordial tensor perturbations and their impact on the present-day spectrum of stochastic gravitational waves. Our main results can be summarized as follows:

1. Primordial magnetogenesis at the end of pseudoscalar inflation can result in sizable present-day magnetic fields with a correlation length on astrophysical scales; see Eqs. (50) and (51). These fields then contribute to the intergalactic magnetic fields we observe today. The main uncertainties in our estimate are: (i) the impact of reheating on the gauge field production after the end of inflation and (ii) the impact of damping effects at temperatures below 10 MeV. In particular, we point out that the presence of a strong hyper-EM field during reheating may open up new channels of particle production, such as pair production via the Schwinger effect. This effect has recently been studied by the authors of Ref. [89], who referred to it as *Schwinger reheating*. Moreover, it is important to understand how the emerging charged plasma back-reacts on the primordial gauge field. A better treatment of this complicated process requires a dedicated numerical simulation that takes into account both nonperturbative particle production as well as MHD effects. Such a study is beyond the scope of this paper; but we certainly encourage further efforts into this direction.

2. The primordial gauge fields generated towards the end of pseudoscalar inflation are maximally helical and can, thus, source the generation of nonzero baryon number around the time of the electroweak crossover via the chiral anomaly in the standard model. We updated previous studies of this mechanism of primordial baryogenesis, which led us to the conclusion that successful baryogenesis is indeed possible in a large part of parameter space, see Eq. (62). We found that the pseudoscalar inflaton must be *weakly* coupled to the hypercharge gauge field, since the primordial gauge fields will otherwise result in an overproduction of baryon number. To be more precise, successful baryogenesis requires an instability parameter ξ of around $\xi \sim 5$ at the end of inflation, which translates into a suppression scale Λ of around $\Lambda \sim 3 \times 10^{17}$ GeV. Again, a main uncertainty of our estimate is the strength of the primordial hypermagnetic field at the time of EWSB. Besides that, the poor knowledge of the temperature dependence of the weak mixing angle during the crossover, $\theta_W(T)$, induces further uncertainties. A better understanding of baryogenesis via decaying helicity, therefore, requires a more careful determination of $\theta_W(T)$.

3. The gauge field production at the end of inflation is accompanied by the production of stochastic gravitational waves. We are able to show that the production of gauge fields consistent with successful baryogenesis at later times typically results a weak GW signal at frequencies in the MHz range or even above; see Eq. (77) and Fig. 7. GWs at such high frequencies are extremely hard to detect; see [90,91] for a past measurement, [92] for an on-going experiment as well as [93,94] for proposals of future techniques. However, if the signal predicted in our scenario should eventually be measured by future experiments, it would serve as a smoking gun for the explosive gauge field production at the end of inflation (and hence provide evidence for baryogenesis via decaying magnetic fields during the electroweak crossover). On the other hand, we are able to conclude that any stronger GW signal would imply the overproduction of baryon number. In this case, one would either have to give up on an inflaton coupling to the standard model hypercharge gauge field or one would have to assume low reheating temperature, such that $T_{\text{rh}} \lesssim T_{\text{ew}}$.

Our analysis illustrates how models of pseudoscalar inflation result in a highly non-trivial interrelation of several, *a priori* unrelated phenomena: the present-day large-scale magnetic field, the baryon asymmetry of the universe, and features in the spectrum of stochastic GWs. In the present paper, we mainly focused on the qualitative aspects of this interplay of phenomena and more work is needed to arrive at more reliable and more precise quantitative predictions. Such an effort requires progress on several fronts. But it also promises to lead to a better understanding of an intriguing cosmological scenario that comes with rich phenomenology deriving from a single additional operator in the effective Lagrangian: $\mathcal{L} \supset a/(4\Lambda) F\tilde{F}$.

Acknowledgements

The authors would like to thank Valerie Domcke, Tomohiro Fujita, Andrew Long, Andreas Ringwald, and Markus Rummel for valuable comments and discussions. K.K. acknowledges support from the DOE for this work under Grant No. DE-SC0013605. This project has received funding from the European Union's Horizon 2020 research and innovation programme under the Marie Skłodowska-Curie grant agreement No. 674896 (K. S.).

References

- [1] B. P. Abbott *et al.* [LIGO Scientific and Virgo Collaborations], *Observation of Gravitational Waves from a Binary Black Hole Merger*, *Phys. Rev. Lett.* **116**, 061102 (2016), 1602.03837 [GR-QC].
- [2] B. P. Abbott *et al.* [LIGO Scientific and Virgo Collaborations], *GW151226: Observation of Gravitational Waves from a 22-Solar-Mass Binary Black Hole Coalescence*, *Phys. Rev. Lett.* **116**, 241103 (2016), 1606.04855 [GR-QC].
- [3] B. P. Abbott *et al.* [LIGO Scientific and VIRGO Collaborations], *GW170104: Observation of a 50-Solar-Mass Binary Black Hole Coalescence at Redshift 0.2*, *Phys. Rev. Lett.* **118**, 221101 (2017), 1706.01812 [GR-QC].
- [4] M. Maggiore, *Gravitational wave experiments and early universe cosmology*, *Phys. Rept.* **331**, 283 (2000), GR-QC/9909001.
- [5] A. A. Starobinsky, *A New Type of Isotropic Cosmological Models Without Singularity*, *Phys. Lett. B* **91**, 99 (1980).
- [6] A. H. Guth, *The Inflationary Universe: A Possible Solution to the Horizon and Flatness Problems*, *Phys. Rev. D* **23**, 347 (1981).
- [7] K. Sato, *First Order Phase Transition of a Vacuum and Expansion of the Universe*, *Mon. Not. Roy. Astron. Soc.* **195**, 467 (1981).
- [8] A. D. Linde, *A New Inflationary Universe Scenario: A Possible Solution of the Horizon, Flatness, Homogeneity, Isotropy and Primordial Monopole Problems*, *Phys. Lett. B* **108**, 389 (1982).
- [9] A. Albrecht and P. J. Steinhardt, *Cosmology for Grand Unified Theories with Radiatively Induced Symmetry Breaking*, *Phys. Rev. Lett.* **48**, 1220 (1982).
- [10] A. A. Starobinsky, *Spectrum of relict gravitational radiation and the early state of the universe*, *JETP Lett.* **30**, 682 (1979), *Pisma Zh. Eksp. Teor. Fiz.* **30**, 719 (1979).

- [11] V. A. Rubakov, M. V. Sazhin and A. V. Veryaskin, *Graviton Creation in the Inflationary Universe and the Grand Unification Scale*, *Phys. Lett.* **115B**, 189 (1982).
- [12] M. Guzzetti, C., N. Bartolo, Liguori, M. and S. Matarrese, *Gravitational waves from inflation*, *Riv. Nuovo Cim.* **39**, 399 (2016), 1605.01615 [ASTRO-PH.CO].
- [13] K. Nakayama, S. Saito, Y. Suwa and J. Yokoyama, *Space laser interferometers can determine the thermal history of the early Universe*, *Phys. Rev. D* **77**, 124001 (2008), 0802.2452 [HEP-PH].
- [14] K. Nakayama, S. Saito, Y. Suwa and J. Yokoyama, *Probing reheating temperature of the universe with gravitational wave background*, *JCAP* **0806**, 020 (2008), 0804.1827 [ASTRO-PH].
- [15] P. A. R. Ade *et al.* [Planck Collaboration], *Planck 2015 results. XX. Constraints on inflation*, *Astron. Astrophys.* **594**, A20 (2016), 1502.02114 [ASTRO-PH.CO].
- [16] B. P. Abbott *et al.* [LIGO Scientific and Virgo Collaborations], *Upper Limits on the Stochastic Gravitational-Wave Background from Advanced LIGO's First Observing Run*, *Phys. Rev. Lett.* **118**, 121101 (2017), 1612.02029 [GR-QC].
- [17] N. Seto, S. Kawamura and T. Nakamura, *Possibility of direct measurement of the acceleration of the universe using 0.1-Hz band laser interferometer gravitational wave antenna in space*, *Phys. Rev. Lett.* **87**, 221103 (2001), ASTRO-PH/0108011.
- [18] S. Kawamura *et al.*, *The Japanese space gravitational wave antenna DECIGO*, *Class. Quant. Grav.* **23**, S125 (2006).
- [19] J. Crowder and N. J. Cornish, *Beyond LISA: Exploring future gravitational wave missions*, *Phys. Rev. D* **72**, 083005 (2005), GR-QC/0506015.
- [20] G. M. Harry, P. Fritschel, D. A. Shaddock, W. Folkner and E. S. Phinney, *Laser interferometry for the big bang observer*, *Class. Quant. Grav.* **23**, 4887 (2006), Erratum *ibid.* **23**, 7361 (2006).
- [21] V. Domcke, M. Pieroni and P. Bintruy, *Primordial gravitational waves for universality classes of pseudoscalar inflation*, *JCAP* **1606**, 031 (2016), 1603.01287 [ASTRO-PH.CO].
- [22] J. Garcia-Bellido, M. Peloso and C. Unal, *Gravitational waves at interferometer scales and primordial black holes in axion inflation*, *JCAP* **1612**, 031 (2016), 1610.03763 [ASTRO-PH.CO].
- [23] J. L. Cook and L. Sorbo, *Particle production during inflation and gravitational waves detectable by ground-based interferometers*, *Phys. Rev. D* **85**, 023534 (2012), Erratum *ibid. D* **86**, 069901 (2012), 1109.0022 [ASTRO-PH.CO].

- [24] M. M. Anber and L. Sorbo, *Non-Gaussianities and chiral gravitational waves in natural steep inflation*, *Phys. Rev. D* **85**, 123537 (2012), 1203.5849 [ASTRO-PH.CO].
- [25] K. Freese, J. A. Frieman and A. V. Olinto, *Natural inflation with pseudo-Nambu-Goldstone bosons*, *Phys. Rev. Lett.* **65**, 3233 (1990).
- [26] F. C. Adams, J. R. Bond, K. Freese, J. A. Frieman and A. V. Olinto, *Natural inflation: Particle physics models, power law spectra for large scale structure, and constraints from COBE*, *Phys. Rev. D* **47**, 426 (1993), HEP-PH/9207245.
- [27] S. Weinberg, *A New Light Boson?*, *Phys. Rev. Lett.* **40**, 223 (1978).
- [28] F. Wilczek, *Problem of Strong p and t Invariance in the Presence of Instantons*, *Phys. Rev. Lett.* **40**, 279 (1978).
- [29] R. D. Peccei and H. R. Quinn, *CP Conservation in the Presence of Instantons*, *Phys. Rev. Lett.* **38**, 1440 (1977).
- [30] R. D. Peccei and H. R. Quinn, *Constraints Imposed by CP Conservation in the Presence of Instantons*, *Phys. Rev. D* **16**, 1791 (1977).
- [31] P. Svrcek and E. Witten, *Axions In String Theory*, *JHEP* **0606**, 051 (2006), HEP-TH/0605206.
- [32] M. B. Green and J. H. Schwarz, *Anomaly Cancellation in Supersymmetric D=10 Gauge Theory and Superstring Theory*, *Phys. Lett.* **149B**, 117 (1984).
- [33] I. Obata, *Chiral primordial blue tensor spectra from the axion-gauge couplings*, 1612.08817 [ASTRO-PH.CO].
- [34] M. S. Turner and L. M. Widrow, *Inflation Produced, Large Scale Magnetic Fields*, *Phys. Rev. D* **37**, 2743 (1988).
- [35] W. D. Garretson, G. B. Field and S. M. Carroll, *Primordial magnetic fields from pseudo-Goldstone bosons*, *Phys. Rev. D* **46**, 5346 (1992), HEP-PH/9209238.
- [36] M. M. Anber and L. Sorbo, *N-flationary magnetic fields*, *JCAP* **0610**, 018 (2006), ASTRO-PH/0606534.
- [37] R. Durrer, L. Hollenstein and R. K. Jain, *Can slow roll inflation induce relevant helical magnetic fields?*, *JCAP* **1103**, 037 (2011), 1005.5322 [ASTRO-PH.CO].
- [38] P. D. Meerburg and E. Pajer, *Observational Constraints on Gauge Field Production in Axion Inflation*, *JCAP* **1302**, 017 (2013), 1203.6076 [ASTRO-PH.CO].
- [39] M. M. Anber and L. Sorbo, *Naturally inflating on steep potentials through electromagnetic dissipation*, *Phys. Rev. D* **81**, 043534 (2010), 0908.4089 [HEP-TH].

- [40] N. Barnaby, R. Namba and M. Peloso, *Phenomenology of a Pseudo-Scalar Inflaton: Naturally Large Nongaussianity*, *JCAP* **1104**, 009 (2011), 1102.4333 [ASTRO-PH.CO].
- [41] N. Barnaby, E. Pajer and M. Peloso, *Gauge Field Production in Axion Inflation: Consequences for Monodromy, non-Gaussianity in the CMB, and Gravitational Waves at Interferometers*, *Phys. Rev. D* **85**, 023525 (2012), 1110.3327 [ASTRO-PH.CO].
- [42] N. Barnaby and M. Peloso, *Large Nongaussianity in Axion Inflation*, *Phys. Rev. Lett.* **106**, 181301 (2011), 1011.1500 [HEP-PH].
- [43] L. Sorbo, *Parity violation in the Cosmic Microwave Background from a pseudoscalar inflaton*, *JCAP* **1106**, 003 (2011), 1101.1525 [ASTRO-PH.CO].
- [44] A. Linde, S. Mooij and E. Pajer, *Gauge field production in supergravity inflation: Local non-Gaussianity and primordial black holes*, *Phys. Rev. D* **87**, 103506 (2013), 1212.1693 [HEP-TH].
- [45] E. Bugaev and P. Klimai, *Axion inflation with gauge field production and primordial black holes*, *Phys. Rev. D* **90**, 103501 (2014), 1312.7435 [ASTRO-PH.CO].
- [46] L. M. Widrow, D. Ryu, D. R. G. Schleicher, K. Subramanian, C. G. Tsagas and R. A. Treumann, *The First Magnetic Fields*, *Space Sci. Rev.* **166**, 37 (2012), 1109.4052 [ASTRO-PH.CO].
- [47] R. Durrer and A. Neronov, *Cosmological Magnetic Fields: Their Generation, Evolution and Observation*, *Astron. Astrophys. Rev.* **21**, 62 (2013), 1303.7121 [ASTRO-PH.CO].
- [48] A. Neronov and I. Vovk, *Evidence for strong extragalactic magnetic fields from Fermi observations of TeV blazars*, *Science* **328**, 73 (2010), 1006.3504 [ASTRO-PH.HE].
- [49] F. Tavecchio, G. Ghisellini, L. Foschini, G. Bonnoli, G. Ghirlanda and P. Coppi, *The intergalactic magnetic field constrained by Fermi/LAT observations of the TeV blazar 1ES 0229+200*, *Mon. Not. Roy. Astron. Soc.* **406**, L70 (2010), 1004.1329 [ASTRO-PH.CO].
- [50] K. Dolag, M. Kachelriess, S. Ostapchenko and R. Tomas, *Lower limit on the strength and filling factor of extragalactic magnetic fields*, *Astrophys. J.* **727**, L4 (2011), 1009.1782 [ASTRO-PH.HE].
- [51] W. Essey, S. Ando and A. Kusenko, *Determination of intergalactic magnetic fields from gamma ray data*, *Astropart. Phys.* **35**, 135 (2011), 1012.5313 [ASTRO-PH.HE].
- [52] A. M. Taylor, I. Vovk and A. Neronov, *Extragalactic magnetic fields constraints from simultaneous GeV-TeV observations of blazars*, *Astron. Astrophys.* **529**, A144 (2011), 1101.0932 [ASTRO-PH.HE].

- [53] K. Takahashi, M. Mori, K. Ichiki, S. Inoue and H. Takami, *Lower Bounds on Magnetic Fields in Intergalactic Voids from Long-term GeV-TeV Light Curves of the Blazar Mrk 421*, *Astrophys. J.* **771**, L42 (2013), 1303.3069 [ASTRO-PH.CO].
- [54] J. D. Finke, L. C. Reyes, M. Georganopoulos, K. Reynolds, M. Ajello, S. J. Fegan and K. McCann, *Constraints on the Intergalactic Magnetic Field with Gamma-Ray Observations of Blazars*, *Astrophys. J.* **814**, no. 1, 20 (2015), 1510.02485 [ASTRO-PH.HE].
- [55] A. Kandus, K. E. Kunze and C. G. Tsagas, *Primordial magnetogenesis*, *Phys. Rept.* **505**, 1 (2011), 1007.3891 [ASTRO-PH.CO].
- [56] M. Giovannini and M. E. Shaposhnikov, *Primordial magnetic fields, anomalous isocurvature fluctuations and big bang nucleosynthesis*, *Phys. Rev. Lett.* **80**, 22 (1998), HEP-PH/9708303.
- [57] M. Giovannini and M. E. Shaposhnikov, *Primordial hypermagnetic fields and triangle anomaly*, *Phys. Rev. D* **57**, 2186 (1998), HEP-PH/9710234.
- [58] K. Bamba, *Baryon asymmetry from hypermagnetic helicity in dilaton hypercharge electromagnetism*, *Phys. Rev. D* **74**, 123504 (2006), HEP-PH/0611152.
- [59] S. H. S. Alexander, M. E. Peskin and M. M. Sheikh-Jabbari, *Leptogenesis from gravity waves in models of inflation*, *Phys. Rev. Lett.* **96**, 081301 (2006), HEP-TH/0403069.
- [60] A. Maleknejad, *Gravitational leptogenesis in axion inflation with $SU(2)$ gauge field*, *JCAP* **1612**, 027 (2016), 1604.06520 [HEP-PH].
- [61] M. M. Anber and E. Sabancilar, *Hypermagnetic Fields and Baryon Asymmetry from Pseudoscalar Inflation*, *Phys. Rev. D* **92**, 101501 (2015), 1507.00744 [HEP-TH].
- [62] T. Fujita and K. Kamada, *Large-scale magnetic fields can explain the baryon asymmetry of the Universe*, *Phys. Rev. D* **93**, 083520 (2016), 1602.02109 [HEP-PH].
- [63] K. Kamada and A. J. Long, *Baryogenesis from decaying magnetic helicity*, *Phys. Rev. D* **94**, 063501 (2016), 1606.08891 [ASTRO-PH.CO].
- [64] K. Kamada and A. J. Long, *Evolution of the Baryon Asymmetry through the Electroweak Crossover in the Presence of a Helical Magnetic Field*, *Phys. Rev. D* **94**, 123509 (2016), 1610.03074 [HEP-PH].
- [65] Y. Cado and E. Sabancilar, *Asymmetric Dark Matter and Baryogenesis from Pseudoscalar Inflation*, 1611.02293 [HEP-PH].
- [66] V. B. Semikoz, A. Y. Smirnov and D. D. Sokoloff, *Generation of hypermagnetic helicity and leptogenesis in the early Universe*, *Phys. Rev. D* **93**, 103003 (2016), 1604.02273 [HEP-PH].

- [67] S. Rostam Zadeh and S. S. Gousheh, *Effects of the $U_Y(1)$ Chern-Simons term and its baryonic contribution on matter asymmetries and hypermagnetic fields*, *Phys. Rev. D* **95**, 056001 (2017), 1607.00650 [HEP-PH].
- [68] A. Brandenburg and K. Subramanian, *Astrophysical magnetic fields and nonlinear dynamo theory*, *Phys. Rept.* **417**, 1 (2005), ASTRO-PH/0405052.
- [69] U. Frisch, A. Pouquet, J. Leorat and A. Mazure, *Possibility of an inverse cascade of magnetic helicity in magnetohydrodynamic turbulence*, *J. Fluid Mech.* **68**, 769 (1975).
- [70] A. Pouquet, U. Frisch and J. Leorat, *Strong MHD helical turbulence and the nonlinear dynamo effect*, *J. Fluid Mech.* **77**, 321 (1976).
- [71] T. Kahniashvili, A. G. Tevzadze, A. Brandenburg and A. Neronov, *Evolution of Primordial Magnetic Fields from Phase Transitions*, *Phys. Rev. D* **87**, 083007 (2013), 1212.0596 [ASTRO-PH.CO].
- [72] A. Vilenkin, *Equilibrium Parity Violating Current In A Magnetic Field*, *Phys. Rev. D* **22**, 3080 (1980).
- [73] R. Banerjee and K. Jedamzik, *The Evolution of cosmic magnetic fields: From the very early universe, to recombination, to the present*, *Phys. Rev. D* **70**, 123003 (2004), ASTRO-PH/0410032.
- [74] P. Adshead and M. Wyman, *Chromo-Natural Inflation: Natural inflation on a steep potential with classical non-Abelian gauge fields*, *Phys. Rev. Lett.* **108**, 261302 (2012), 1202.2366 [HEP-TH].
- [75] P. Adshead, E. Martinec and M. Wyman, *Perturbations in Chromo-Natural Inflation*, *JHEP* **1309**, 087 (2013), 1305.2930 [HEP-TH].
- [76] P. Adshead, J. T. Giblin, T. R. Scully and E. I. Sfakianakis, *Magnetogenesis from axion inflation*, *JCAP* **1610**, 039 (2016), 1606.08474 [ASTRO-PH.CO].
- [77] P. Adshead, J. T. Giblin, T. R. Scully and E. I. Sfakianakis, *Gauge-preheating and the end of axion inflation*, *JCAP* **1512**, 034 (2015), 1502.06506 [ASTRO-PH.CO].
- [78] T. Fujita, R. Namba, Y. Tada, N. Takeda and H. Tashiro, *Consistent generation of magnetic fields in axion inflation models*, *JCAP* **1505**, 054 (2015), 1503.05802 [ASTRO-PH.CO].
- [79] P. Fileviez Perez and H. H. Patel, *The Electroweak Vacuum Angle*, *Phys. Lett. B* **732**, 241 (2014), 1402.6340 [HEP-PH].
- [80] M. Abramowitz and I. Stegun, *Handbook of Mathematical Functions with Formulas, Graphs, and Mathematical Tables*, Dover, New York (1972).

- [81] M. Gedalin, *Linear waves in relativistic anisotropic magnetohydrodynamics*, [Phys. Rev. E](#) **47**, 4354 (1993).
- [82] G. Baym and H. Heiselberg, *The Electrical conductivity in the early universe*, [Phys. Rev. D](#) **56**, 5254 (1997), [ASTRO-PH/9704214](#).
- [83] P. B. Arnold, G. D. Moore and L. G. Yaffe, *Transport coefficients in high temperature gauge theories. 1. Leading log results*, [JHEP](#) **0011**, 001 (2000), [HEP-PH/0010177](#).
- [84] M. D’Onofrio, K. Rummukainen and A. Tranberg, *Sphaleron Rate in the Minimal Standard Model*, [Phys. Rev. Lett.](#) **113**, 141602 (2014), [1404.3565](#) [[HEP-PH](#)].
- [85] M. D’Onofrio and K. Rummukainen, *Standard model cross-over on the lattice*, [Phys. Rev. D](#) **93**, 025003 (2016), [1508.07161](#) [[HEP-PH](#)].
- [86] K. Kajantie, M. Laine, K. Rummukainen and M. E. Shaposhnikov, *A Nonperturbative analysis of the finite T phase transition in $SU(2) \times U(1)$ electroweak theory*, [Nucl. Phys. B](#) **493**, 413 (1997), [HEP-LAT/9612006](#).
- [87] P. A. R. Ade *et al.* [Planck Collaboration], *Planck 2015 results. XIII. Cosmological parameters*, [Astron. Astrophys.](#) **594**, A13 (2016), [1502.01589](#) [[ASTRO-PH.CO](#)].
- [88] W. Buchmuller, V. Domcke, K. Kamada and K. Schmitz, *The Gravitational Wave Spectrum from Cosmological $B-L$ Breaking*, [JCAP](#) **1310**, 003 (2013), [1305.3392](#) [[HEP-PH](#)].
- [89] W. Tangarife, K. Tobioka, L. Ubaldi and T. Volansky, *Dynamics of Relaxed Inflation*, [1706.03072](#) [[HEP-PH](#)].
- [90] A. Nishizawa *et al.*, *Laser-interferometric Detectors for Gravitational Wave Background at 100 MHz: Detector Design and Sensitivity*, [Phys. Rev. D](#) **77**, 022002 (2008), [0710.1944](#) [[GR-QC](#)].
- [91] T. Akutsu *et al.*, *Search for a stochastic background of 100-MHz gravitational waves with laser interferometers*, [Phys. Rev. Lett.](#) **101**, 101101 (2008), [0803.4094](#) [[GR-QC](#)].
- [92] A. S. Chou *et al.* [Holometer Collaboration], *MHz Gravitational Wave Constraints with Decameter Michelson Interferometers*, [Phys. Rev. D](#) **95**, 063002 (2017), [1611.05560](#) [[ASTRO-PH.IM](#)].
- [93] A. M. Cruise, *The potential for very high-frequency gravitational wave detection*, [Class. Quant. Grav.](#) **29**, 095003 (2012).
- [94] A. Arvanitaki and A. A. Geraci, *Detecting high-frequency gravitational waves with optically-levitated sensors*, [Phys. Rev. Lett.](#) **110**, 071105 (2013), [1207.5320](#) [[GR-QC](#)].